Figure 9 (revised)

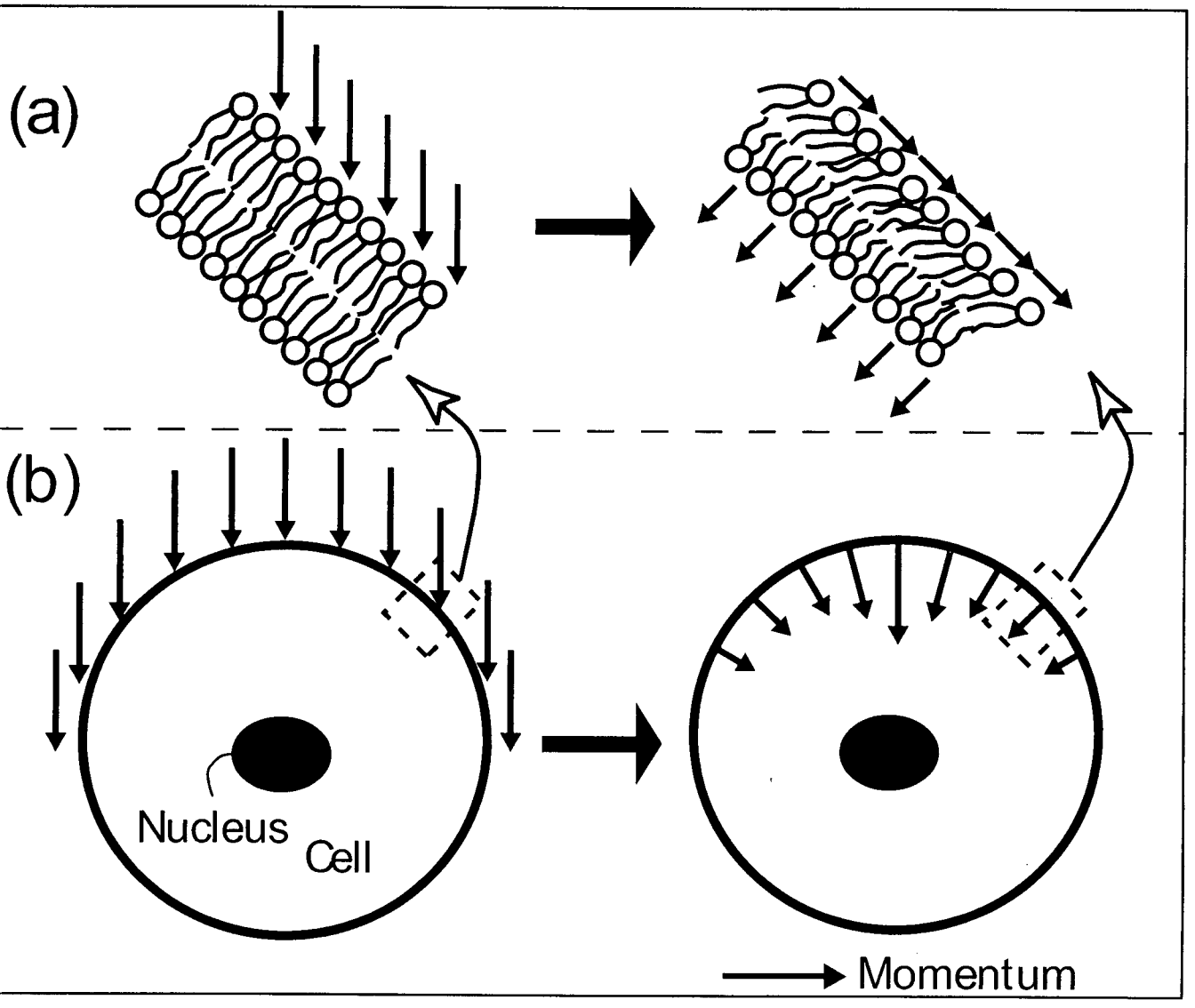

British Journal of Cancer (2007) 97, 170 – 176

www.bjcancer.com

Clinical Studies

# A phase I and pharmacokinetic study of NK105, a paclitaxel-incorporating micellar nanoparticle formulation

**T Hamaguchi*[,1], K Kato[1], H Yasui[1], C Morizane[1], M Ikeda[1], H Ueno[1], K Muro[1], Y Yamada[1], T Okusaka[1], K Shirao[1], Y Shimada[1], H Nakahama[2] and Y Matsumura[3]**

*[1]Department of Medicine National Cancer Center Hospital, 5-1-1 Tsukiji, Chuo-ku, Tokyo 104-0045, Japan; [2]Clinical Trial Coordinating Division, National Cancer Center Hospital, 5-1-1 Tsukiji, Chuo-ku, Tokyo 104-0045, Japan; [3]Investigative Treatment Division, Research Center for Innovative Oncology, National Cancer Center Hospital East, 6-5-1 Kashiwanoha, Kashiwa, 277-8577, Japan*

This phase I study was designed to examine the maximum tolerated dose (MTD), the dose-limiting toxicities (DLTs), the recommended dose (RD) for phase II, and the pharmacokinetics of NK105, a new polymeric micelle carrier system for paclitaxel (PTX). NK105 was administered as a 1-h intravenous infusion every 3 weeks, without antiallergic premedication. The starting dose was 10 mg m$^{-2}$, and the dose was escalated according to the accelerated titration method. Nineteen patients were recruited. The tumour types treated included pancreatic ($n = 11$), bile duct ($n = 5$), gastric ($n = 2$), and colonic ($n = 1$) cancers. Neutropenia was the most common haematological toxicity. A grade 3 fever developed in one patient given 180 mg m$^{-2}$. No other grades 3 or 4 nonhaematological toxicities, including neuropathy, was observed during the entire study period. DLTs occurred in two patients given 180 mg m$^{-2}$ (grade 4 neutropenia lasting for more than 5 days). Thus, this dose was designated as the MTD. Grade 2 hypersensitivity reactions developed in only one patient given 180 mg m$^{-2}$. A partial response was observed in one patient with pancreatic cancer. The maximum concentration ($C_{max}$) and area under the concentration (AUC) of NK105 were dose dependent. The plasma AUC of NK105 at 150 mg m$^{-2}$ was approximately 15-fold higher than that of the conventional PTX formulation. NK105 was well tolerated, and the RD for the phase II study was determined to be 150 mg m$^{-2}$ every 3 weeks. The results of this phase I study warrant further clinical evaluation.

*British Journal of Cancer* (2007) **97,** 170 – 176. doi:10.1038/sj.bjc.6603855 www.bjcancer.com
Published online 26 June 2007


**Keywords:** NK105; paclitaxel; polymer micelles; phase I study; DDS

Paclitaxel (PTX), an antimicrotubule agent, has a wide spectrum of antitumour activity including ovarian, breast, stomach, lung, and head and neck cancers (Rowinsky *et al*, 1990; Carney, 1996; Crown and O'Leary, 2000). The clinically used PTX preparation is a mixture of Cremophor EL and ethanol because of PTX's poor water solubility. However, the use of Cremophor EL is known to be associated with acute hypersensitivity reactions (Weiss *et al*, 1990; Rowinsky and Donehower, 1995; Kloover *et al*, 2004). Other PTX preparations that have been categorised as drug delivery systems (DDS) have also been developed. These preparations include Xyotax (polyglutamate-conjugated PTX; Singer *et al*, 2003; Boddy *et al*, 2005), Abraxane (PTX coated with albumin; Ibrahim *et al*, 2002; Deisai *et al*, 2003; Nyman *et al*, 2005), and Genexol-PM (a PTX micelle in which PTX has been simply solubilised; Kim *et al*, 2004). The common advantage shared by these formulations is that they are injectable intravenously without the mixture of Cremophor EL and ethanol. Among them, Abraxane has been approved for metastatic breast cancer by the Food and Drug Administration in the USA based on the results of a randomised phase 3 trial. In this trial, Abraxane demonstrated significantly higher response rates, compared with standard PTX, and a significantly longer time to progression (Gradishar *et al*, 2005). In addition, the incidence of grade 4 neutropenia was significantly lower for Abraxane than for PTX. However, peripheral sensory neuropathy was more common in the arm (Gradishar *et al*, 2005).

NK105 is a PTX-incorporating 'core-shell-type' polymeric micellar nanoparticle formulation (Hamaguchi *et al*, 2005). This particle can be injected intravenously without the use of Cremophor EL or ethanol as a vehicle. Therefore, NK105 is expected to possess a clinical advantage similar to that of the above-mentioned PTX formulations. The difference between NK105 and the other PTX dosage forms is that NK105 is expected to yield a markedly higher plasma and tumour area under the concentration (AUC), compared with those for the other PTX formulations. Moreover, regarding the toxic profiles, the repeated administration of NK105 to rats at 7-day intervals produced significantly fewer toxic effects on peripheral nerves than free PTX. Macromolecular drugs, including NK105, have been developed based on the characteristic macroscopic features of solid tumours, such as hypervasculature, the presence of vascular permeability factors stimulating extravasation within cancer, and the suppressed lymphatic clearance of macromolecules. These characteristics, which are unique to solid tumours, constitute the basis of the enhanced permeability and retention (EPR) effect (Matsumura and Maeda, 1986; Maeda *et al*, 2000; Duncan, 2003). The *in vivo*

*Correspondence: Dr T Hamaguchi; E-mail: thamaguc@ncc.go.jp
Received 13 March 2007; revised 23 May 2007; accepted 23 May 2007; published online 26 June 2007

antitumour activity of NK105 was significantly more potent than that of free PTX, probably because of enhanced tumour exposure through the EPR effect (Hamaguchi *et al*, 2005).

We conducted a phase I clinical trial using NK105 in patients with advanced solid tumours. The objectives of this trial were to determine the maximum tolerated dose (MTD), the phase II recommended dose (RD), and the pharmacokinetics of NK105.

## PATIENTS AND METHODS

The protocol and all materials were approved by the Institutional Review Board of the National Cancer Center, Tokyo. This study was conducted in compliance with the Good Clinical Practice Guidelines of the International Conference on Harmonization and the Declaration of Helsinki Principles. Written informed consent was obtained from all the patients.

### Therapeutic agent

NK105 was supplied by Nippon Kayaku Co. Ltd. (Tokyo, Japan) in 20-ml glass vials containing a dose equivalent to 30 mg of PTX. When reconstituted in 10 ml of 5% glucose solution and diluted with a total volume of 250 ml of 5% glucose, the reconstituted solution was stable for 24 h at room temperature. In our preclinical study, DLS and HPLC analysis showed that less than 2% of PTX incorporated in the micelles was released for 24 h at room temperature (data not shown).

Figure 1 shows the schematic structure of NK105, a PTX-entrapped polymeric micelle formulation. The NK105 polymers were constructed using polyethylene glycol (PEG) as the hydrophilic component and modified polyaspartate as the hydrophobic component. PEG is believed to form the outer shell of the micelle, producing a 'stealth' effect that enables NK105 to avoid being captured by the reticuloendothelial system.

The modified polyaspartate chain is hydrophobic and is believed to form the hydrophobic inner core of the micelles in aqueous media. The hydrophobic inner core enables NK105 to entrap a sufficient amount of PTX. NK105 has a diameter of about 90 nm (Hamaguchi *et al*, 2005).

### Patients

Patients with solid tumours refractory to conventional chemotherapy and for whom no effective therapy was available were eligible for enrolment in this study, provided that the following criteria were met: a histologically confirmed malignant tumour; a performance status of $\leqslant 2$; an age of $\geqslant 20$ and $<75$ years; a normal haematological profile (neutrophil count $\geqslant 2000\,mm^{-3}$, platelet count $\geqslant 100\,000\,mm^{-3}$, hemoglobin $\geqslant 9\,g\,dl^{-1}$); normal hepatic function (total bilirubin level $\leqslant 1.5\,mg\,dl^{-1}$, AST and ALT $\leqslant 2.5$ times the upper normal limit); normal renal function (serum creatinine $\leqslant 1.5\,mg\,dl^{-1}$); normal cardiac function (New York Heart Association (NYHA) classification of $\leqslant 1$); normal pulmonary function ($PaO_2 \geqslant 60$ mm Hg); no chemotherapy within 4 weeks (6 weeks for nitrosourea or mitomycin C) of the administration of NK105; and a life expectancy of more than 2 months. Patients with serious infections (including hepatitis B, hepatitis C, or HIV) were ineligible for enrolment in the study. Patients who had been previously treated with a taxane were excluded because of assessing neuropathy. Patients were also excluded if they were pregnant or lactating. Additionally, any patient whom the investigators considered ineligible was excluded.

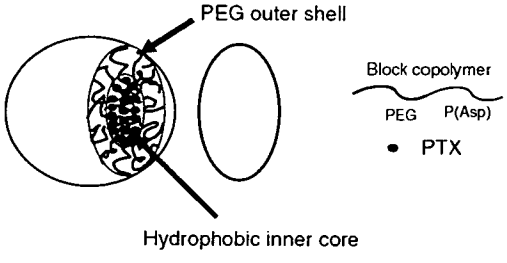


**Figure 1** Schematic structure of NK105. A polymeric micelle carrier of NK105 consists of a block copolymer of PEG (molecular weight of about 12 000) and modified polyaspartate. PEG is believed to be the outer shell of the micelle. PEG is believed to form the outer shell of the micelle. NK105 has a highly hydrophobic inner core, and therefore can entrap a sufficient amount of PTX.

### Drug administration

NK105 was dissolved in 5% glucose solution for injection at room temperature. NK105 was administered intravenously without in-line filtration and without premedication. NK105 solution was infused using an electric pump at a speed of $250\,ml\,h^{-1}$.

### Dosage and dose escalation

The starting dosage of NK105 was $10\,mg\,m^{-2}$, which is one-third of the toxic dose low in dogs. NK105 was administered once every 3 weeks, and the treatment was continued unless a severe adverse event or disease progression was observed. Dose escalation was performed according to the previously described accelerated titration method (Simon *et al*, 1997; Matsumura *et al*, 2004).

Toxicity was graded from 1 to 4 using the National Cancer Institute Common Toxicity Criteria (version 2.0). Intrapatient dose escalation was not permitted. The MTD was defined as the level at which two out of six patients experienced dose-limiting toxicities (DLTs). The recommended dosage for a phase II trial was defined by the Efficacy and Safety Assessment Committee based on the safety, pharmacokinetics, and efficacy results of this trial. DLT was defined as grade 4 neutropenia lasting more than 5 days, a platelet count of less than $25\,000\,\mu l^{-1}$, or grade 3 or higher non-haematological toxicity, with the exception of nausea, vomiting, appetite loss, and hypersensitivity.

### Pretreatment assessment and follow-up care

A complete medical history and physical examination, performance status evaluation, complete blood cell count (CBC), blood chemistry, urinalysis, electrocardiogram (ECG), and a computed tomography (CT) examination were performed in each patient. Other examinations were performed only in the presence of a specific clinical indication. Patients were physically examined every day until the second administration of NK105; CBC and blood chemistry tests were performed on day 3 and weekly thereafter. An ECG examination was repeated before each administration of NK105. Tumour marker levels were also measured before every administration. Tumour response was evaluated according to the Response Evaluation Criteria in Solid Tumors criteria (Therasse *et al*, 2000).

### Liquid chromatography/tandem mass spectrometry determination of PTX concentrations

The PTX concentrations determined in the present phase I study represented the total drug concentrations (both micelle-entrapped and released). It was difficult to measure released PTX and micelle-entrapped PTX separately, because the equilibrium between both forms could not keep constant during the separating procedure. PTX was extracted from human plasma (0.2 ml) or urine (0.5 ml) by deproteinisation with acetonitrile. The quantifications of PTX in plasma and urine were performed using liquid chromatography/tandem mass spectrometry. Reversed-phase column-switching

chromatography was conducted using an ODS column and detection was enabled by electrospray ionisation of positive mode.

### Pharmacokinetic analysis

The following pharmacokinetic parameters were calculated for each patient using a non-compartmental model using the WinNonlin Professional version 4.1 program (Pharsight Corporation, Mountain View, CA, USA). The maximum concentration ($C_{max}$) was the maximum observed plasma concentration of PTX, and the time-to-the-maximum concentration ($T_{max}$) was the time corresponding to $C_{max}$. The area under the concentration (AUC)-time curve from time zero up to the last quantifiable time point ($AUC_{0-t}$) was calculated using the linear trapezoidal rule, and the area under the concentration-time curve from zero until infinity ($AUC_{0-inf.}$) was calculated as the sum of $AUC_{0-t}$ and the extrapolated area under the zero moment curve from the last quantifiable time point to infinity calculated by dividing the plasma concentration of the last quantifiable time point (observed value) by the elimination rate constant. The half-life of the terminal phase ($t_{1/2z}$) was calculated as $\log_e 2/\lambda z$, where $\lambda z$ is the elimination rate constant calculated from the terminal linear portion of the log of the concentration in plasma. Total clearance ($CL_{tot}$), the volume of distribution at steady state ($V_{ss}$), and renal clearance ($CL_r$) were calculated using the following equations, where $D$ is the dose and $AUMC_{inf.}$ the area under the first moment curve from time zero until infinity:

$$CL_{tot} = D/AUC_{inf.}$$

$$V_{ss} = AUMC_{inf.}/AUC_{inf.} \times CL_{tot}$$

$$CL_r = \text{cumulative urinary excretion}/AUC_{inf.} / \text{body surface area}$$

## RESULTS

### Patient characteristics

Nineteen eligible patients were recruited for the study (Table 1). All the patients had received chemotherapy before enrolment. Prior therapies ranged from 1 to 3 regimens of chemotherapy. None of the patients had received taxane chemotherapy. All the patients were included in the safety and response analyses.

### Dosing

Dosage escalation started at 10 mg m$^{-2}$ and was increased up to 180 mg m$^{-2}$. In total, 73 administrations were performed in 19 patients. Eighteen patients received more than two administrations. The maximum number of treatments was 14 courses at 150 mg m$^{-2}$; the average number of administrations at all levels was 3.8 courses. Up until 80 mg m$^{-2}$, grade 2 toxicity was not observed during the first course.

According to the original protocol, the dosage of NK105 should have been doubled for each escalation until grade 2 toxicity. However, the safety committee recommended that the dosage should be raised by 40% instead of 100% at 110 mg m$^{-2}$ and that a modified Fibonacci escalation method should be implemented. Therefore, we recruited three patients at dosage level 5 (110 mg m$^{-2}$) and re-started the dose identification study using a modified Fibonacci method.

**Table 1** Patient characteristics

| | |
|---|---|
| Number of patients | 19 |
| Male/female | 13/6 |
| *Age (years)* | |
| Median | 57 |
| Range | 43–72 |
| *ECOG PS* | |
| Median | 0 |
| 0 | 10 |
| 1 | 9 |
| *Prior treatment* | |
| Chemotherapy regimens | |
| Median | 1 |
| Range | 1–3 |

### Haematological toxicity

Significant myelosuppression was not observed up to level 4 (80 mg m$^{-2}$). At level 7 (180 mg m$^{-2}$), two out of five patients appeared to have acquired DLTs, namely grade 4 neutropenia lasting for more than 5 days. On the basis of these results, 180 mg m$^{-2}$ was considered to be the MTD, with neutropenia as the DLT. Since a dosage of 150 mg m$^{-2}$ was considered to be the recommended dosage for phase II studies, an additional four patients were enrolled at a dosage of 150 mg m$^{-2}$; one patient developed DLT, namely grade 4 neutropenia lasting for more than 5 days (Table 2). During the entire period of this study, G-CSF was never used to rescue patients.

### Nonhaematological toxicity

The NK105 injection was generally uneventful and well tolerated in terms of nonhaematological toxicities (Table 2). Most of the toxicities were grade 1; none of the patients manifested grade 4 toxicity. A few patients developed a grade 1 elevation in AST or ALT, but these changes were transient. Pain or local toxicity in the area of the injection was not observed in any of the patients treated with NK105. No infusion-related reactions were observed; such reactions sometimes occur during liposomal drug administration. Patients were not premedicated with steroids or antihistamines. Only one patient at 180 mg m$^{-2}$ developed grade 2 hypersensitivity. After the first course, the patient received premedication of hydrocortisone and did not develop such hypersensitivity after that. The other 18 patients did not experience any hypersensitivity during the study. Neuropathy occurred in a typical stocking/glove distribution and was manifested by numbness. Three patients at level 6 (150 mg m$^{-2}$) and three patients at level 7 (180 mg m$^{-2}$) experienced grade 1 neurotoxicity during 1 cycle. Of the four patients who received multicycle treatment more than five times, only three patients developed grade 2 neuropathy and the other patient developed grade 1 neuropathy. Even one patient who received 14 cycles of treatment experienced only grade 2 neuropathy.

### Pharmacokinetics

The plasma concentrations of PTX after the intravenous infusion of NK105 were determined in each of the patients enrolled at a dose of 150 mg m$^{-2}$ (Figure 2A). The $C_{max}$ (Figure 2B) and AUC (Figure 2C) increased as the doses were escalated from 10 to 180 mg m$^{-2}$. The pharmacokinetic parameters are summarised in Table 3. The $t_{1/2Z}$ ranged from 7.0 to 13.2 h, and a slight tendency towards a dose-dependent extension of this parameter was observed. The $CL_{tot}$ ranged from 280.9 to 880.4 ml h$^{-1}$ m$^{-2}$, and the $V_{ss}$ ranged from 3668.9 to 10 400.3 ml m$^{-2}$. Although these parameters were slightly reduced depending on the dose, linear pharmacokinetics was assumed to have been observed in the dose range from 10 to 180 mg m$^{-2}$. The AUC of NK105 at 150 mg m$^{-2}$ (recommended phase II dose) was about 15-fold larger than that of conventional PTX at dose of 210 mg m$^{-2}$ (conventional dose for a

**Table 2** Haematological and nonhaematological toxicities (cycle 1 and all cycles)

| | 10–110 mg m$^{-2}$ ($n=7$) grade | | | | 150 mg m$^{-2}$ ($n=7$) grade | | | | 180 mg m$^{-2}$ ($n=7$) grade | | | |
|---|---|---|---|---|---|---|---|---|---|---|---|---|
| | 1 | 2 | 3 | 4 | 1 | 2 | 3 | 4 | 1 | 2 | 3 | 4 |
| *Cycle 1* | | | | | | | | | | | | |
| Leukopenia | 2 | 0 | 2 | 0 | 1 | 5 | 1 | 0 | 1 | 1 | 3 | 0 |
| Neutropenia | 1 | 0 | 1 | 1 | 0 | 2 | 1 | 3[a] | 0 | 0 | 3 | 2[b] |
| Thrombocytopenia | 1 | 0 | 0 | 0 | 2 | 0 | 0 | 0 | 4 | 0 | 0 | 0 |
| Hemoglobin | 1 | 0 | 0 | 0 | 2 | 2 | 0 | 0 | 1 | 0 | 0 | 0 |
| Neuropathy | 0 | 0 | 0 | 0 | 3 | 0 | 0 | 0 | 3 | 0 | 0 | 0 |
| Myalgia | 1 | 0 | 0 | 0 | 3 | 0 | 0 | 0 | 2 | 1 | 0 | 0 |
| Arthralgia | 1 | 0 | 0 | 0 | 4 | 0 | 0 | 0 | 3 | 0 | 0 | 0 |
| Hypersensitivity | 0 | 0 | 0 | 0 | 0 | 0 | 0 | 0 | 0 | 1 | 0 | 0 |
| Rash | 1 | 0 | 0 | 0 | 1 | 3 | 0 | 0 | 4 | 0 | 0 | 0 |
| Fatigue | 1 | 0 | 0 | 0 | 5 | 0 | 0 | 0 | 4 | 0 | 0 | 0 |
| Fever | 2 | 0 | 0 | 0 | 2 | 0 | 0 | 0 | 1 | 0 | 1 | 0 |
| Anorexia | 0 | 0 | 0 | 0 | 3 | 0 | 0 | 0 | 1 | 0 | 0 | 0 |
| Nausea | 1 | 0 | 0 | 0 | 1 | 0 | 0 | 0 | 1 | 0 | 0 | 0 |
| Stomatitis | 0 | 0 | 0 | 0 | 1 | 0 | 0 | 0 | 1 | 0 | 0 | 0 |
| Alopecia | 3 | 0 | — | — | 5 | 0 | — | — | 5 | 0 | — | — |
| *All cycles* | | | | | | | | | | | | |
| Leukopenia | 3 | 0 | 2 | 0 | 1 | 4 | 2 | 0 | 1 | 1 | 3 | 0 |
| Neutropenia | 1 | 0 | 1 | 1 | 1 | 1 | 1 | 4 | 0 | 0 | 3 | 2 |
| Thrombocytopenia | 1 | 0 | 0 | 0 | 3 | 0 | 0 | 0 | 4 | 0 | 0 | 0 |
| Hemoglobin | 1 | 0 | 0 | 0 | 1 | 5 | 0 | 0 | 1 | 0 | 0 | 0 |
| Neuropathy | 2 | 0 | 0 | 0 | 1 | 3 | 0 | 0 | 4 | 0 | 0 | 0 |
| Myalgia | 1 | 1 | 0 | 0 | 3 | 0 | 0 | 0 | 2 | 1 | 0 | 0 |
| Arthralgia | 2 | 0 | 0 | 0 | 4 | 0 | 0 | 0 | 3 | 0 | 0 | 0 |
| Hypersensitivity | 0 | 0 | 0 | 0 | 0 | 0 | 0 | 0 | 0 | 1 | 0 | 0 |
| Rash | 1 | 0 | 0 | 0 | 3 | 3 | 0 | 0 | 4 | 0 | 0 | 0 |
| Fatigue | 3 | 0 | 0 | 0 | 5 | 1 | 0 | 0 | 4 | 0 | 0 | 0 |
| Fever | 3 | 0 | 0 | 0 | 3 | 1 | 0 | 0 | 1 | 0 | 1 | 0 |
| Anorexia | 2 | 1 | 0 | 0 | 2 | 1 | 0 | 0 | 2 | 0 | 0 | 0 |
| Nausea | 1 | 0 | 0 | 0 | 1 | 0 | 0 | 0 | 2 | 0 | 0 | 0 |
| Stomatitis | 1 | 0 | 0 | 0 | 2 | 0 | 0 | 0 | 1 | 0 | 0 | 0 |
| Alopecia | 2 | 2 | — | — | 4 | 3 | — | — | 4 | 1 | — | — |

[a]One of three patients developed DLT, namely grade 4 neutropenia lasting for more than 5 days. [b]These two patients developed DLT, namely grade 4 neutropenia lasting for more than 5 days.

3-week regimen in Japanese patients) (Tamura *et al*, 1995). The $V_{ss}$ and $CL_{tot}$ of NK105 were significantly lower than those of conventional PTX.

The cumulative urinary excretion rates of PTX (0–73 h) after the administration of NK105 were 2.8–9.2%. These values were low, similar to those reported after the administration of conventional PTX (Tamura *et al*, 1995). The $CL_r$ ranged from 11.7 to 66.4 ml h$^{-1}$ m$^{-3}$, and was slightly decreased with the dose. Since the ratio of $CL_r$ to $CL_{tot}$ was 3–9%, $CL_r$ hardly contributed to $CL_{tot}$.

## Therapeutic response

Six patients (two gastric, two bile duct, one colon, and one pancreatic) were evaluated as having had a stable disease for longer than 4 weeks at the time of the study's completion. A partial response was seen in a patient with metastatic pancreatic cancer who had been treated at 150 mg m$^{-2}$, and in whom the size of the liver metastasis had decreased by more than 90%, compared to the baseline scan (Figure 3A). This patient had previously undergone treatment with gemcitabine. The antitumour response was maintained for nearly 1 year. In a patient with stomach cancer who was treated at 150 mg m$^{-2}$, about 40% reduction was observed in a peritoneal metastasis, but a liver metastasis remained stable (Figure 3B).

## DISCUSSION

The observed toxicities of NK105 were similar to those expected for conventional PTX. The DLT was neutropenia. The recommended phase II dose using a 3-week schedule was determined to be 150 mg m$^{-2}$. This recommended dose of NK105 is less than that of conventional PTX (210 mg m$^{-2}$). Since the plasma AUC of the recommended dose of NK105 was 15- to 20-fold higher than that of the recommended dose of conventional PTX (210 mg m$^{-2}$), whether the so-called therapeutic window of NK105 is wider than that of conventional PTX should be determined in a future phases II or III trial, although the therapeutic window of NK105 appears to be wider than that of free PTX in mice experiments (Hamaguchi *et al*, 2005).

In general, haematological toxicity was mild and well managed in this trial. PTX is known to cause cumulative peripheral neuropathy resulting in the discontinuation of treatment with PTX. At a dose of 150 mg m$^{-2}$, three out of seven patients experienced only grade 1 neuropathy during the first cycle. Since the patients enrolled in this trial had almost intractable cancer, such as pancreatic or stomach, a relatively small number of patients received multiple cycles of treatment. Therefore, NK105-related neurotoxicity could not be evaluated in this study. However, three out of four patients who received more than five cycles of treatment experienced transient grade 2 peripheral neuropathy, and other patient developed transient grade 1 peripheral neuropathy. Future phase II trials may clarify whether NK105 is less toxic in terms of peripheral neuropathy when compared with conventional PTX, Abraxane, and other PTX compounds. Another characteristic adverse effect of PTX is hypersensitivity, which may be mainly caused by Cremophor EL. Since NK105 is not formulated in a Cremophor EL-containing solvent, we presumed that hypersensitivity would be diminished.

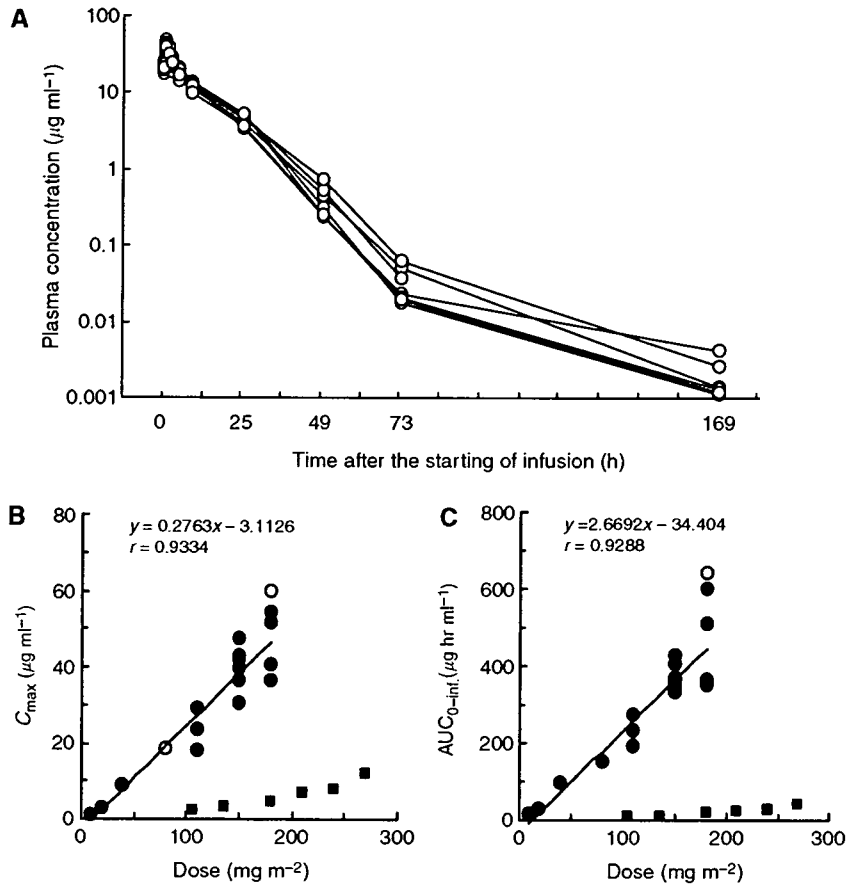


**Figure 2** (**A**) Individual plasma concentrations of PTX in seven patients following 1-h intravenous infusion of NK105 at a dose of 150 mg m$^{-2}$. (**B**) Relationships between dose and $C_{max}$, and (**C**) between dose and $AUC_{0-inf.}$ of PTX in patients following 1-h intravenous infusion of NK105. Regression analysis for dose *vs* $C_{max}$ was applied using all points except one patient at 80 mg m$^{-2}$ whose medication time became 11 min longer and one patient at 180 mg m$^{-2}$ who had medication discontinuation and steroid medication. (Plots were shown as open circle). Regression analysis for dose *vs* $AUC_{0-inf.}$ was applied using all points except one patient who had medication discontinuation and steroid medication. (Plot was shown as open circle.) Relationships between dose and $C_{max}$, and $AUC_{0-inf.}$ in patients following conventional PTX administration were plotted (closed square, see Tamura *et al*, 1995).

**Table 3** Pharmacokinetic parameters

| | Dose (mg m$^{-2}$) | *n* | $C_{max}$ (μg ml$^{-1}$) | $AUC_{0-inf.}$ (μg h ml$^{-1}$) | $t_{1/2}$ (h) | $CL_{tot}$ (ml h$^{-1}$ m$^{-2}$) | $V_{ss}$ (ml m$^{-2}$) | UE[a] (%) | $CL_r$ (ml h m$^{-2}$) |
|---|---|---|---|---|---|---|---|---|---|
| NK105 | 10 | 1 | 0.9797 | 11.4 | 9 | 880.4 | 10400.3 | 7.5 | 66.4 |
| | 20 | 1 | 2.8971 | 29.1 | 8.5 | 687.9 | 8027 | 8.6 | 59.4 |
| | 40 | 1 | 8.8334 | 93.9 | 13.2 | 426.1 | 5389.8 | 5.2 | 22 |
| | 80 | 1 | 18.4533 | 149.3 | 7 | 535.8 | 5875.8 | 4.7 | 25.3 |
| | 110 | 3 | 23.3924 | 232 | 9.7 | 483.3 | 5881.2 | 7.6 | 35.6 |
| | | | ±5.6325 | ±39.1 | ±1.6 | ±82.7 | ±1512.0 | ±1.7 | ±6.9 |
| | 150 | 7 | 40.1699 | 369.8 | 10.6 | 408.6 | 4527.1 | 5.3 | 21.6 |
| | | | ±5.5334 | ±35.2 | ±1.3 | ±37.3 | ±639.5 | ±1.5 | ±6.5 |
| | 180 | 4[b] | 45.6278 | 454.5 | 11.3 | 416.5 | 4983.4 | 5.9 | 23.7 |
| | | | ±8.6430 | ±119.1 | ±0.6 | ±104.7 | ±887.5 | ±1.4 | ±4.2 |

[a]UE, urinary excretion. [b]One patient at 180 mg m$^{-2}$ level was omitted from the calculation of summary pharmacokinetic parameters, as there was administrating interruption for developing allergic reactions.

Indeed, the results of this clinical trial show that NK105 can be administered safely as a short infusion (1 h) without the administration of antiallergic agents like dexamethasone and antihistamine, although one patient at 180 mg m$^{-2}$ developed transient grade 2 hypersensitivity at the first course. Therefore, NK105 may offer advantages in terms of safety and patient convenience and comfort.

The pharmacokinetic analysis of NK105 suggests that the distribution of PTX-incorporating micelles is mostly restricted to the plasma and, in part, to extracellular fluids in the body. This is consistent with data obtained in a preclinical study (Hamaguchi *et al*, 2005) showing that the distribution of NK105 in tissues is characterised by an EPR effect, similar to that of tumour and inflammatory lesions, or by the presence of a reticuloendothelial

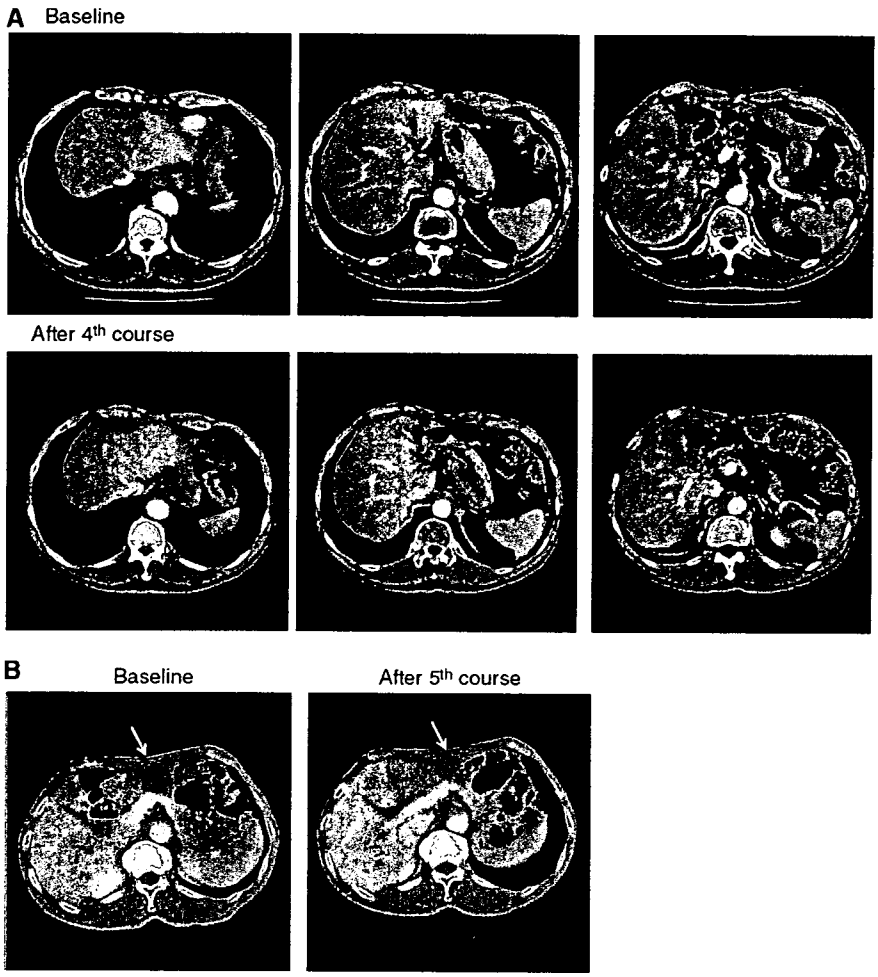


**Figure 3** Serial CT scans. (**A**) A 60-year-old male with pancreatic cancer who was treated with NK105 at a dose level of 150 mg m$^{-2}$. Baseline scan (upper panels) showing multiple metastasis in the liver. Partial response, characterized by a more than 90% decrease in the size of the liver metastasis (lower panels) compared with the baseline scan. The antitumour response was maintained for nearly 1 year. (**B**) A 64-year-old male with stomach cancer who was treated with NK105 at a dose level of 150 mg m$^{-2}$. Baseline scan (left panel) showing a peritoneal metastasis and liver metastasis. About 40% reduction (right panel) was observed in peritoneal metastasis, but not in the liver metastasis after fifth course.

**Table 4** Pharmacokinetic parameters

| | Dose (mg m$^{-2}$) | *n* | $C_{max}$ ($\mu$g ml$^{-1}$) | $AUC_{0-inf.}$ ($\mu$g h$^{-1}$ ml$^{-1}$) | $t_{1/2}$ (h) | $CL_{tot}$ (ml h$^{-1}$ m$^{-2}$) | $V_{ss}$ (ml m$^{-2}$) | UE (%) | $CL_r$ (ml h m$^{-2}$) |
|---|---|---|---|---|---|---|---|---|---|
| NK105 | 150 | 7 | 40.1699 | 369.8 | 10.6 | 408.6 | 4527.1 | 5.3 | 21.6 |
| | | | ±5.5334 | ±35.2 | ±1.3 | ±37.3 | ±639.5 | ±1.5 | ±6.5 |
| PTX | 210 | 5 | 6.744 | 23.18 | 13.3 | 10740 | 58 900 | 9.45 | 1020 |
| | | | ±2.733 | ±10.66 | ±1.5 | ±4860 | ±24 700 | ±3.76 | ±648 |
| XYOTAX[a] | 233 | 4 | NA | 1583 | 120 | 276 | 6200 | NA | NA |
| | | | | ±572 | ±28 | ±63 | ±2100 | | |
| Abraxane | 300 | 5 | 13.52 | 17.61 | 14.6 | 17 700 | 370 000 | NA | NA |
| | | | ±0.95 | ±3.70 | ±2.04 | ±3894 | ±85 100 | | |
| Genoxol-PM | 300 | 3 | 3.107 | 11.58 | 11.4 | 29 300 | NA | NA | NA |
| | | | ±1.476 | ±4.28 | ±2.4 | ±13 800 | | | |

[a]Conjugated taxanes.

system. When compared with conventional PTX at a dose of 210 mg m$^{-2}$ (conventional dose for a 3-week regimen in Japanese patients), NK105 at a dose of 150 mg m$^{-2}$ (recommended phase II dose) exhibited more than 15-fold larger plasma AUC and a 26-fold lower $CL_{tot}$. The larger plasma AUC is consistent with the stability of the micelle formulation in plasma. The $V_{ss}$ of NK105 was 13-fold lower than that of conventional PTX. This suggests that PTX may have a relatively lower distribution in normal tissue, including normal neural tissue, following NK105 administration. Regarding the drug distribution in tumours, nanoparticle drug carriers have been known to preferentially accumulate in tumour tissues utilising the EPR effect (Matsumura and Maeda, 1986;

Maeda *et al*, 2000; Duncan, 2003). We speculate that NK105 accumulates more in tumour tissues than free PTX, since NK105 is very stable in the circulation and exhibits a markedly higher plasma AUC than free PTX. Moreover, a polymeric micelle carrier system for a drug has the potential to enable the sustained release of the drug inside a tumour following the accumulation of micelles in the tumour tissue (Hamaguchi *et al*, 2005; Uchino *et al*, 2005; Koizumi *et al*, 2006). Regarding NK105 in particular, this sustained release may begin at a PTX-equivalent dose of $<1\,\mu g\,ml^{-1}$ (data not shown). Consequently, the released PTX is distributed throughout the tumour tissue where it kills the cancer cells directly.

In the present study, NK105 appeared to exhibit characteristic pharmacokinetics different from those of other PTX formulations including conventional PTX, Abraxane, Genexol-PM, and Xyotax. For example, previous clinical PK data at each phase II recommended dose shown that plasma AUC and $C_{max}$ were 11.58 and 3.1 in Genexol-PM (Table 4). The antitumour activities seen in two patients with intractable cancers are encouraging. In addition, we recently demonstrated in preclinical study that combined NK105 chemotherapy with radiation exerts a significantly more potent antitumour activity, compared with combined PTX therapy and radiation (Negishi *et al*, 2006). This data on NK105 justifies its continued clinical evaluation.

Clinical Studies

## ACKNOWLEDGEMENTS

We thank the patients who participated in this trial. We also thank Kaoru Shiina and Hiromi Orita for their secretarial assistance.

## REFERENCES

Boddy AV, Plummer ER, Todd R, Sludden J, Griffin M, Robson L, Cassidy J, Bissett D, Bernareggi A, Verrill MW, Calvert AH (2005) A phase I and pharmacokinetic study of paclitaxel poliglumex (XYOTAX), investigating both 3-weekly and 2-weekly schedules. *Clin Cancer Res* **11**: 7834–7840

Carney DN (1996) Chemotherapy in the management of patients with inoperable non-small cell lung cancer. *Semin Oncol* **23**: 71–75

Crown J, O'Leary M (2000) The taxanes: an update. *Lancet* **355**: 1176–1178

Deisai N, Trieu V, Yao R (2003) Evidence of greater antitumor activity of Cremophor-free nanoparticle albumin-bound (nab) paclitaxel (Abraxane) compared to Taxol, role of a novel albumin transporter mechanism. *26th Annual San Antonio Breast Cancer Symposium* San Antonio, TX

Duncan R (2003) The dawning era of polymer therapeutics. *Nat Rev Drug Discov* **2**: 347–360

Gradishar WJ, Tjulandin S, Davidson N, Shaw H, Desai N, Bhar P, Hawkins M, O'Shaughnessy J (2005) Phase III trial of nanoparticle albumin-bound paclitaxel compared with polyethylated castor oil-based paclitaxel in women with breast cancer. *J Clin Oncol* **23**: 7794–7803

Hamaguchi T, Matsumura Y, Suzuki M, Shimizu K, Goda R, Nakamura I, Nakatomi I, Yokoyama M, Kataoka K, Kakizoe T (2005) NK105, a paclitaxel-incorporating micellar nanoparticle formulation, can extend *in vivo* antitumour activity and reduce the neurotoxicity of paclitaxel. *Br J Cancer* **92**: 1240–1246

Ibrahim NK, Desai N, Legha S, Soon-Shiong P, Theriault RL, Rivera E, Esmaeli B, Ring SE, Bedikian A, Hortobagyi GN, Ellerhorst JA (2002) Phase I and pharmacokinetic study of ABI-007, a Cremophor-free, protein-stabilized, nanoparticle formulation of paclitaxel. *Clin Cancer Res* **8**: 1038–1044

Kim TY, Kim DW, Chung JY, Shin SG, Kim SC, Heo DS, Kim NK, Bang YJ (2004) Phase I and pharmacokinetic study of Genexol-PM, a cremophor-free, polymeric micelle-formulated paclitaxel, in patients with advanced malignancies. *Clin Cancer Res* **10**: 3708–3716

Kloover JS, den Bakker MA, Gelderblom H, van Meerbeeck JP (2004) Fatal outcome of a hypersensitivity reaction to paclitaxel: a critical review of premedication regimens. *Br J Cancer* **90**: 304–305

Koizumi F, Kitagawa M, Negishi T, Onda T, Matsumoto S, Hamaguchi T, Matsumura Y (2006) Novel SN-38-incorporating polymeric micelles, NK012, eradicate vascular endothelial growth factor-secreting bulky tumors. *Cancer Res* **66**: 10048–10056

Maeda H, Wu J, Sawa T, Matsumura Y, Hori K (2000) Tumor vascular permeability and the EPR effect in macromolecular therapeutics: a review. *J Control Release* **65**: 271–284

Matsumura Y, Maeda H (1986) A new concept for macromolecular therapeutics in cancer chemotherapy: mechanism of tumoritropic accumulation of proteins and the antitumor agent smancs. *Cancer Res* **46**: 6387–6392

Matsumura Y, Hamaguchi T, Ura T, Muro K, Yamada Y, Shimada Y, Shirao K, Okusaka T, Ueno H, Ikeda M, Watanabe N (2004) Phase I clinical trial and pharmacokinetic evaluation of NK911, a micelle-encapsulated doxorubicin. *Br J Cancer* **91**: 1775–1781

Negishi T, Koizumi F, Uchino H, Kuroda J, Kawaguchi T, Naito S, Matsumura Y (2006) NK105, a paclitaxel-incorporating micellar nanoparticle, is a more potent radiosensitising agent compared to free paclitaxel. *Br J Cancer* **95**: 601–606

Nyman DW, Campbell KJ, Hersh E, Long K, Richardson K, Trieu V, Desai N, Hawkins MJ, Von Hoff DD (2005) Phase I and pharmacokinetics trial of ABI-007, a novel nanoparticle formulation of paclitaxel in patients with advanced nonhematologic malignancies. *J Clin Oncol* **23**: 7785–7793

Rowinsky EK, Donehower RC (1995) Paclitaxel (taxol). *New Engl J Med* **332**: 1004–1014

Rowinsky EK, Cazenave LA, Donehower RC (1990) Taxol: a novel investigational antimicrotubule agent. *J Natl Cancer Inst* **82**: 1247–1259

Simon R, Freidlin B, Rubinstein L, Arbuck SG, Collins J, Christian MC (1997) Accelerated titration designs for phase I clinical trials in oncology. *J Natl Cancer Inst* **89**: 1138–1147

Singer JW, Baker B, De Vries P, Kumar A, Shaffer S, Vawter E, Bolton M, Garzone P (2003) Poly-(L)-glutamic acid-paclitaxel (CT-2103) [XYOTAX], a biodegradable polymeric drug conjugate: characterization, preclinical pharmacology, and preliminary clinical data. *Adv Exp Med Biol* **519**: 81–99

Tamura T, Sasaki Y, Nishiwaki Y, Saijo N (1995) Phase I study of paclitaxel by three-hour infusion: hypotension just after infusion is one of the major dose-limiting toxicities. *Jpn J Cancer Res* **86**: 1203–1209

Therasse P, Arbuck SG, Eisenhauer EA, Wanders J, Kaplan RS, Rubinstein L, Verweij J, Van Glabbeke M, van Oosterom AT, Christian MC, Gwyther SG (2000) New guidelines to evaluate the response to treatment in solid tumors. European Organization for Research and Treatment of Cancer, National Cancer Institute of the United States, National Cancer Institute of Canada. *J Natl Cancer Inst* **92**: 205–216

Uchino H, Matsumura Y, Negishi T, Koizumi F, Hayashi T, Honda T, Nishiyama N, Kataoka K, Naito S, Kakizoe T (2005) Cisplatin-incorporating polymeric micelles (NC-6004) can reduce nephrotoxicity and neurotoxicity of cisplatin in rats. *Br J Cancer* **93**: 678–687

Weiss RB, Donehower RC, Wiernik PH, Ohnuma T, Gralla RJ, Trump DL, Baker Jr JR, Van Echo DA, Von Hoff DD, Leyland-Jones B (1990) Hypersensitivity reactions from taxol. *J Clin Oncol* **8**: 1263–1268

# Novel SN-38–Incorporated Polymeric Micelle, NK012, Strongly Suppresses Renal Cancer Progression

Makoto Sumitomo,[1] Fumiaki Koizumi,[2] Takako Asano,[1] Akio Horiguchi,[1] Keiichi Ito,[1] Tomohiko Asano,[1] Tadao Kakizoe,[3] Masamichi Hayakawa,[1] and Yasuhiro Matsumura[4]

[1]Department of Urology, National Defense Medical College, Tokorozawa, Saitama, Japan; [2]Shien-Lab, Medical Oncology, National Cancer Center Hospital; [3]National Cancer Center, Tokyo, Japan; and [4]Investigative Treatment Division, Research Center for Innovative Oncology, National Cancer Center Hospital East, Chiba, Japan

## Abstract

**It has been recently reported that NK012, a 7-ethyl-10-hydroxy-camptothecin (SN-38)–releasing nanodevice, markedly enhances the antitumor activity of SN-38, especially in hypervascular tumors through the enhanced permeability and retention effect. Renal cell carcinoma (RCC) is a typical hypervascular tumor with an irregular vascular architecture. We therefore investigated the antitumor activity of NK012 in a hypervascular tumor model from RCC. Immunohistochemical examination revealed that Renca tumors contained much more CD34-positive neovessels than SKRC-49 tumors. Compared with CPT-11, NK012 had significant antitumor activity against both bulky Renca and SKRC-49 tumors. Notably, NK012 eradicated rapid-growing Renca tumors in 6 of 10 mice, whereas it failed to eradicate SKRC-49 tumors. In the pulmonary metastasis treatment model, an enhanced and prolonged distribution of free SN-38 was observed in metastatic lung tissues but not in nonmetastatic lung tissues after NK012 administration. NK012 treatment resulted in a significant decrease in metastatic nodule number and was of benefit to survival. Our study shows the outstanding advantage of polymeric micelle-based drug carriers and suggests that NK012 would be effective in treating disseminated RCCs with irregular vascular architectures.** [Cancer Res 2008;68(6):1631–5]

## Introduction

Passive targeting of the drug delivery system is suited to combating the pathophysiologic characteristics present in many solid tumors: hypervascularity, irregular vascular architecture, potential for secretion of vascular permeability factors, and the absence of effective lymphatic drainage that prevents efficient clearance of macromolecules. These characteristics, unique to solid tumors, are believed to be the basis of the enhanced permeability and retention (EPR) effect (1). Polymeric micelle-based anticancer drugs have recently been developed (2, 3), and some were put under evaluation for clinical trials (4, 5).

7-Ethyl-10-hydroxy-camptothecin (SN-38), a biological active metabolite of irinotecan hydrochloride (CPT-11), has potent antitumor activity, but has not been used clinically because it is a water-insoluble drug. It has been recently shown that novel SN38-incorporated polymeric micelles, NK012, have the potential to allow effective sustained release of SN-38 inside a tumor and possess potent antitumor activities especially in a vascular endothelial growth factor (VEGF)–secreting hypervascular tumor (6), because the supramolecular structures of NK012 which enable SN-38 to accumulate in the target tissue are based on the EPR effect (1).

Renal cell carcinoma (RCC) is a typical hypervascular tumor with an irregular vascular architecture. We therefore conducted an investigation to determine whether NK012 would be effective in treating RCC by using established RCC tumor models with pulmonary metastasis.

## Materials and Methods

**Drugs and cells.** CPT-11 was purchased from Yakult Honsha Co., Ltd. SN-38 and NK012 was prepared and supplied by Nippon Kayaku Co., Ltd. (6). Five human RCC lines (SKRC-49, Caki-1, 769P, 786O, and KU19-20) and murine Renca cells were maintained in DMEM or MEM supplemented with 2 mmol/L glutamine, 1% nonessential amino acids, 100 units/mL streptomycin and penicillin, and 10% FCS.

***In vitro* growth inhibition assay.** The growth inhibitory effects of NK012, SN-38, and CPT-11 were examined with a 3-(4, 5-dimethylthiazol-2-yl)-2, 5-diphenyltetrazolium bromide (MTT) assay, as described previously (6).

***In vivo* growth inhibition assay.** The animal experimental protocols were approved by the Committee for Ethics of Animal Experimentation, and the experiments were conducted in accordance with the Guidelines for Animal Experiments in the National Cancer Center. Athymic nude mice (3–4 wk old) were maintained in a laminar air flow cabinet under aseptic conditions. $10^7$ RCC cells were s.c. injected into the backs of the mice. NK012 at doses of 10 mg/kg/d or 20 mg/kg/d and CPT-11 at doses of 15 mg/kg/d or 30 mg/kg/d were given i.v. on days 0 (when tumors were allowed to grow until they became massive in size, around 1.5 cm), 4, and 8. Tumor volume was determined by direct measurement with calipers and calculated as $\pi/6 \times$ (large diameter) $\times$ (small diameter)$^2$.

**Assessment of treatment effects of NK012 on murine pulmonary metastasis model.** A total of $1 \times 10^5$ Renca cells were inoculated into male BALB/c mice via the tail vein. The mice were randomly divided into three groups of 10. NK012 at dose of 20 mg/kg/d and CPT-11 at dose of 30 mg/kg/d were given i.v. on days 0 (7 d after inoculation), 4, and 8. After that, the mice were sacrificed, their lungs were stained intratracheally with 15% India black ink solution, and the number of metastatic nodules in each mouse was counted. To determine the effect of NK012 on survival, an identical experiment to the one described above was done. After treatment, mice were maintained until each animal showed signs of morbidity (i.e., over 10% weight loss compared with untreated controls), at which point they were sacrificed. Kaplan-Meier analysis was done to determine the effect on time to morbidity, and statistical differences were ranked according to a Mantel-Cox log-rank test using the StatView 5.0 software package.

**Histologic and immunohistochemical analysis.** Histologic sections were taken from Renca tumor tissues. After extirpation, tissues were fixed with 3.9% formalin in PBS (pH 7.4), and the subsequent preparations and H&E staining were performed by Tokyo Histopathological Laboratory Co.,

**Requests for reprints:** Yasuhiro Matsumura, Investigative Treatment Division, Research Center for Innovative Oncology, National Cancer Center Hospital East, 6-5-1 Kashiwanoha, Kashiwa City, Chiba 277-8577, Japan. Phone: 81-4-7134-6857; Fax: 81-4-7134-6857; E-mail: yhmatsum@east.ncc.go.jp.



doi:10.1158/0008-5472.CAN-07-6532

**Table 1.** *In vitro* growth inhibitory activity of SN-38, NK012, and CPT-11 in RCC lines (MTT assay)

| Cell line | $IC_{50}$ (μmol/L) | | |
|---|---|---|---|
| | SN-38 | NK012* | CPT-11 |
| SKRC-49 | 0.0064 ± 0.005 | 0.011 ± 0.008 | 4.14 ± 0.45 |
| Caki-1 | 0.0062 ± 0.009 | 0.032 ± 0.006 | 8.45 ± 0.85 |
| 769P | 0.015 ± 0.007 | 0.085 ± 0.014 | 34.54 ± 3.76 |
| 786O | 0.031 ± 0.007 | 0.12 ± 0.012 | 28.14 ± 1.21 |
| KU19-20 | 0.10 ± 0.006 | 0.34 ± 0.014 | 32.65 ± 1.25 |
| Renca | 0045 ± 0.005 | 0.0096 ± 0.008 | 2.26 ± 0.05 |

*The dose of NK012 is expressed as a dose equivalent to SN-38.

Ltd. Monoclonal anti-CD34 antibody (HyCult Biotechnology) was used to detect the tumor blood vessels. CD34-positive neovessels were counted in 10 high-power fields (×400) by two independent investigators who operated in a blinded fashion.

**Assay for free (polymer-unbound) SN-38 in lung tissues.** The Renca pulmonary metastasis model described above was used for the analysis of the biodistribution of NK012 and CPT-11. Ten days after Renca inoculation, NK012 (20 mg/kg) or CPT-11 (30 mg/kg) was given i.v. to the mice. The mice were sacrificed at 0, 24, 48, and 72 h after administration, and lung samples were taken and stored at −80°C until analysis. We prepared control mice without Renca inoculation as the nonmetastatic model; NK012 was administrated as well, and lung samples were stored. Samples were then homogenized on ice using a Digital homogenizer (Iuchi) and suspended in the mixture of 100 mmol/L glycine-HCl buffer (pH 3)/methanol (1:1, v/v) at a concentration of 5% w/w. Proteins were precipitated with an ice-cold mixture of 1 mmol/L $H_3PO_4$/MeOH/$H_2O$ (1:1:4, v/v/v) containing camptothecin as an I.S. The sample was vortexed for 10 s and filtered through a MultiScreen Solvinert (Millipore Corporation), and the concentration of free SN-38 in the aliquots of the homogenates (100 μL) was determined using the high-performance liquid chromatography method (6).

**Statistical analysis.** Data were expressed as mean ± SD. Significance of differences was calculated using the unpaired *t* test with repeated measures of StatView 5.0. $P < 0.05$ was regarded as statistically significant.

## Results and Discussion

We first evaluated *in vitro* cellular sensitivity of RCC lines to SN-38, NK012, and CPT-11. The $IC_{50}$ values of each agent for RCC lines are shown in Table 1. NK012 exhibited higher cytotoxic effect against each cell line compared with CPT-11 (96-fold to 406-fold sensitive).

It is essential to elucidate the correlation between the effectiveness of micellar drugs and tumor hypervascularity and hyperpermeability. Gross evaluation of those RCC tumors s.c. injected into the backs of mice revealed that Renca tumors were more reddish and grew faster than SKRC-49 tumors, and immunohistochemical examination showed that Renca tumors contained much more CD34-positive neovessels than SKRC-49 tumors (Fig. 1).

We allowed the tumors to grow until they became massive, around 1.5 cm, and then initiated treatment. A striking decrease in Renca tumor volume was observed on day 15 in mice treated with NK012 at 20 mg/kg/d compared with the untreated control (Fig. 2*A*). Renca bulky masses completely disappeared on day 21 in 6 of 10 mice treated with NK012 at 20 mg/kg/d. On the other hand, Renca tumors in mice treated with CPT-11 at 30 mg/kg/d were not eradicated and rapidly regrew after a partial response at day 15. An approximate 10% body weight loss occurred in mice treated with NK012 20 mg/kg, compared with the untreated controls, but there was no significant difference in comparison with tumor-free mice treated with NK012, suggesting that the decrease in body weight was likely to be due to tumor shrinkage rather than toxic effects. We next compared the antitumor activities of the NK012 and CPT-11 treatment in SKRC-49 and Renca tumors. The SKRC-49 tumor volume in mice treated with NK012 at 20 mg/kg/d on day 21 was over 70% smaller than in the untreated controls on day 21 and ~50% smaller than in mice on day 0 (Fig. 2*B*). However, the SKRC-49 tumors were not eradicated in mice treated with NK012. Considering that equivalent *in vitro* growth inhibitory effects by NK012 were observed for SKRC-49 and Renca cells (Table 1), our results suggest that the antitumor activity of NK012 *in vivo* might be affected by tumor environment factors, such as tumor vascularity.

We next examined the distribution of free SN-38 in the metastatic or nonmetastatic (no inoculation of Renca cells) lung tissues after administration of NK012 or CPT-11. In the case of NK012 administration in mice with lung metastasis, free SN-38 was detectable at the concentration of >100 ng/g in metastatic lung tissues with a typical microvascular architecture (Fig. 3*A*) even at 72 hours after administration, whereas the concentrations of free SN-38 in nonmetastatic lung tissues after NK012 administration were much lower than those in metastatic lung tissues after treatment with NK012 (significant at 24, 48, and 72 hours; $P < 0.05$;

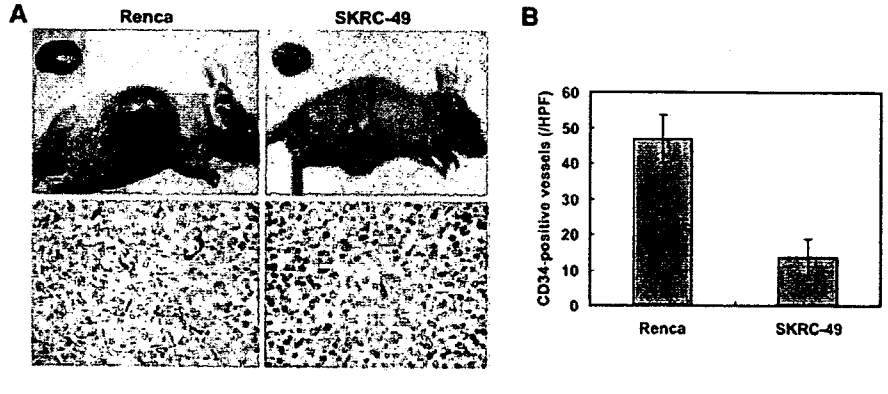


**Figure 1.** Comparison of tumor angiogeneses of Renca and SKRC-49 in athymic nude mice. *A*, representative photographs of massive tumors developed from Renca and SKRC-49 at 28 d after s.c. injection (inoculation). Immunohistochemical (CD34, ×400) examinations for each tumor are shown. *B*, tumor neovascularization in each tumor was quantified by counting CD34-positive neovessels. *Bars*, SD. Experiments were repeated twice with similar results.

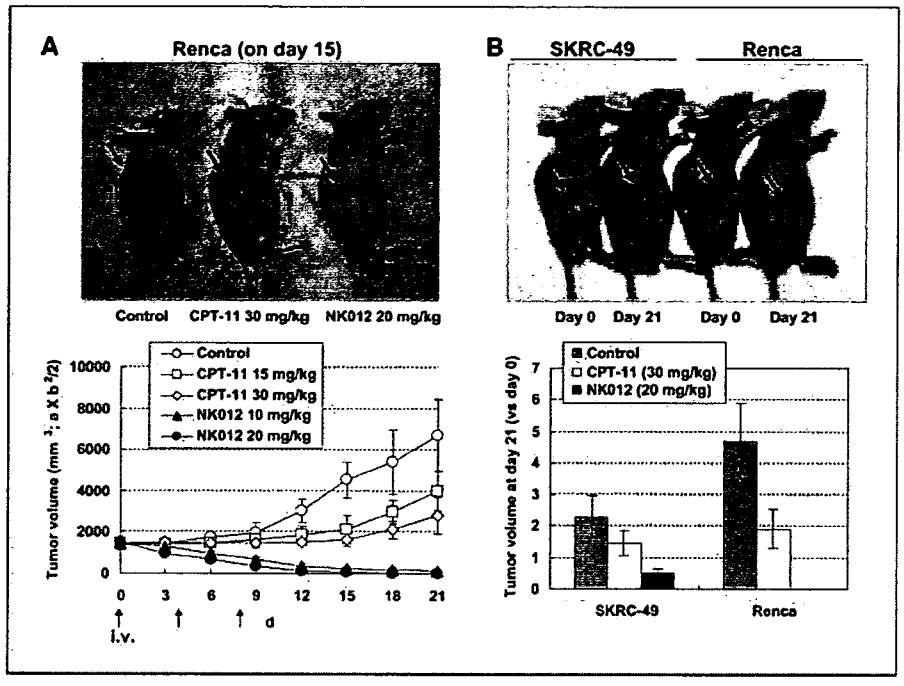


**Figure 2.** Growth-inhibitory effect of NK012 and CPT-11 on bulky RCC tumors. I.v. administration of NK012 or CPT-11 was started when the mean tumor volumes of groups reached a massive 1,500 $mm^3$. The mice were divided into test groups as indicated. *A*, representative of each group at day 15 in the Renca allograft model. *Arrows*, Renca allografts (*top*). Time profile of tumor volume in mice treated with NK012 or CPT-11 at indicated doses (*bottom*). Each group consisted of 10 mice. *Bars*, SD. *B*, the comparison of antitumor activities of CPT-11 and NK012 in SKRC-49 xenografts and Renca allografts. Representative of mice treated with NK012 at day 0 and day 21. Experiments were repeated twice with similar results. The mice at day 0 in the photograph belong to the group in the second experiment which started just at day 21 of the first experiment. *Arrows*, tumor grafts. The relative tumor volume values at day 21 to those at day 0 in each group set to 1 (*bottom*). Each group consisted of 10 mice.

Fig. 3*B*). On the other hand, the concentrations of free SN-38 after administration of CPT-11 were almost negligible in metastatic lung tissues at all time points (data not shown). These results strongly suggest that SN-38 could be selectively released from NK012 and maintained in metastatic Renca tumor tissues.

Deviating from the ordinary experimental pulmonary metastasis prevention model, we initiated treatment 7 days after inoculation (day 0) when multiple lung nodules derived from Renca were observed in all mice in our preliminary study (Fig. 4*A*). On day 21, there was no significant difference between the mean number of metastatic nodules in the control group (287 ± 56 nodules, $n = 10$) and in the group receiving CPT-11 treatment (236 ± 59 nodules, $n = 10$). Significant treatment effects were found, however, in the group receiving NK012 treatment (32 ± 18 nodules, $n = 10$) on day 21 compared with the control group on day 21 ($P < 0.0001$). Notably, a dramatic decrease in metastatic nodule number was observed in the NK012 treatment group on day 21 compared with the control group on day 0 (126 ± 23 nodules, $n = 10$, $P < 0.001$; Fig. 4*A*). Kaplan-Meier analysis showed that a significant survival benefit was obtained in the NK012 treatment group compared with

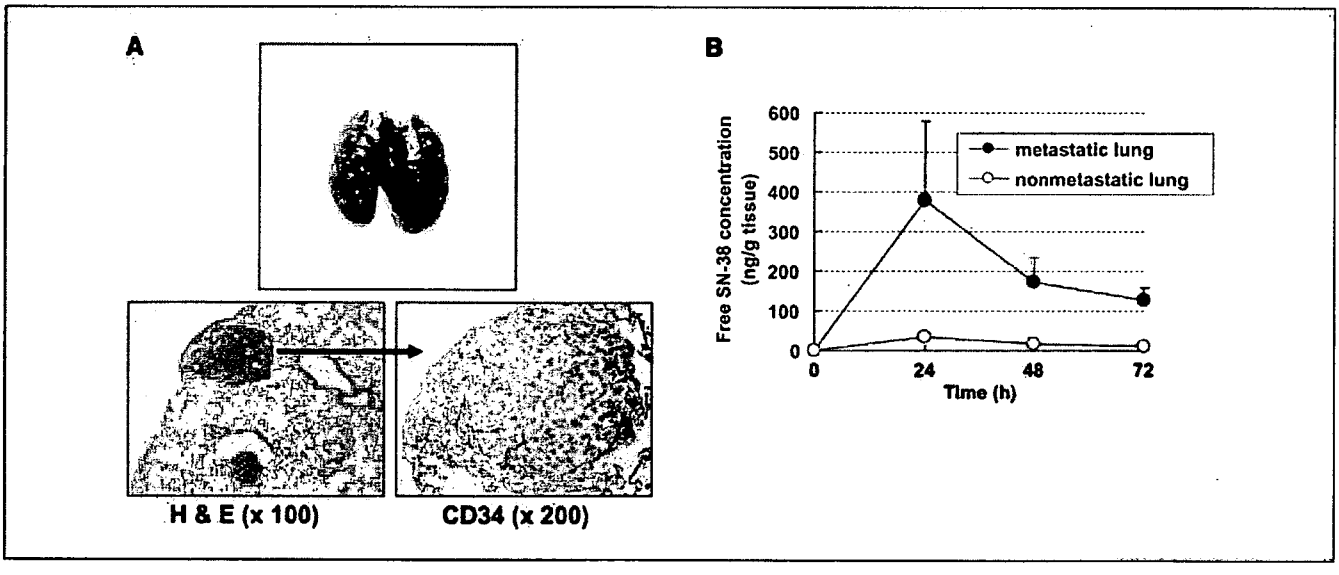


**Figure 3.** Pulmonary metastasis of Renca cells and lung tissue distribution of free SN-38 after administration of NK012 and CPT-11. *A*, gross appearances of pulmonary metastasis observed 7 d after Renca inoculation (*top*). Multiple metastatic nodules and neovascularization in metastatic lung tumor lesion (*bottom*). *B*, time profile of free SN-38 concentration in metastatic or nonmetastatic lung tissues in mice treated with NK012 (20 mg/kg/d). *Bars*, SD. Experiments were performed in tetraplicate.

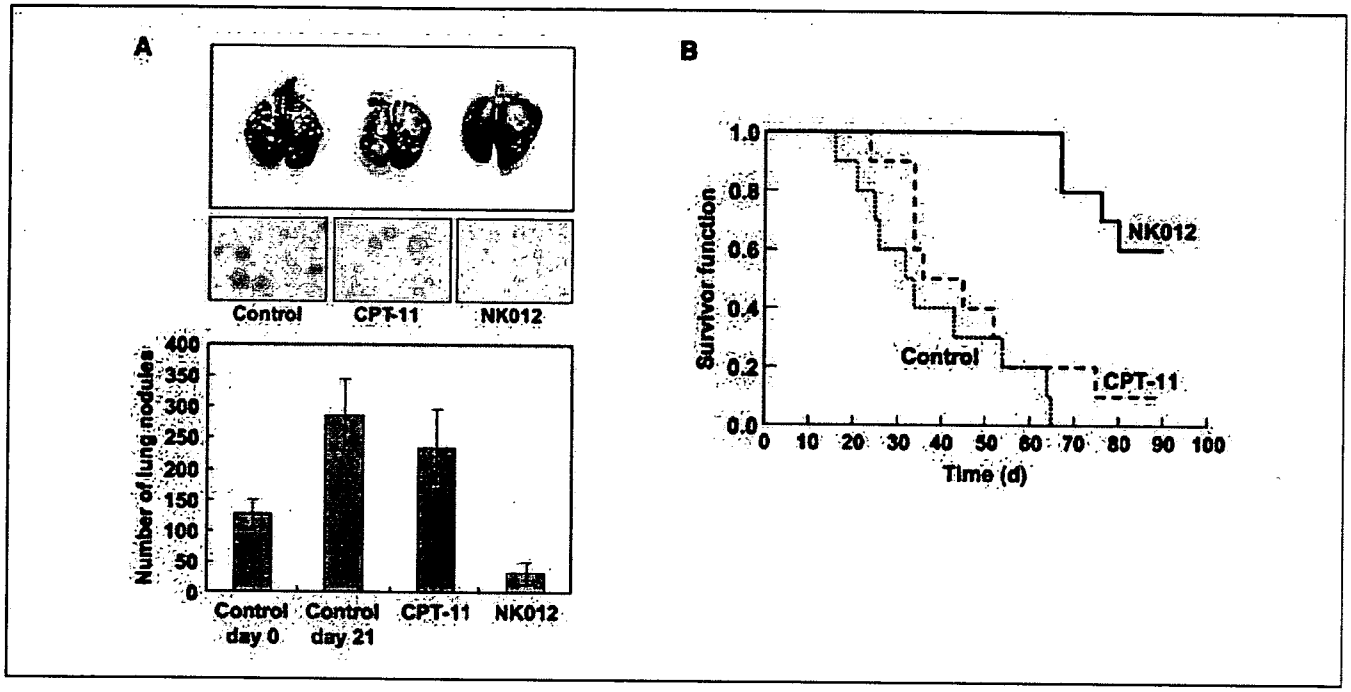


**Figure 4.** Treatment effect of NK012 on established pulmonary metastasis and survival. NK012 (20 mg/kg/d) and CPT-11 (30 mg/kg/d) were given i.v. to mice with established pulmonary metastasis on days 0 (7 d after Renca inoculation), 4, and 8. *A*, gross and histologic appearances of pulmonary metastases at day 21 (*top*). The metastatic nodules in each mouse were counted. Each group consisted of five mice. *B*, mice were maintained for 90 d after each treatment and survival was assessed by a Kaplan-Meier analysis. Each group consisted of five mice. Experiments were repeated twice with similar results.

the control group ($P < 0.001$), but no significant survival benefit was obtained in CPT-11 treatment group ($P = 0.239$; Fig. 4*B*). Although no severe toxic effects were observed in any mouse treated with NK012, 3 of 10 mice treated with NK012 were sacrificed during the observation period according to the 'Guidelines for Animal Experiments because their body weights had become 10% lower than those of the other mice. However, the sacrificed mice were a little bit smaller than others when they started treatment, and they showed no disseminated lung metastasis (data not shown).

Our results presented here strongly support recent findings reported by us that the macromolecular drug distribution throughout the tumor site was enhanced by the hypervascularity and hyperpermeability, and subsequently higher antitumor activity was achieved (6). We assume that conventional low molecular size anticancer agents almost disappear from the bloodstream without being subjected to the EPR effect before they can reach the target organs (solid tumor). The clinical importance of angiogenesis in human tumors has been shown in several reports indicating a positive relationship between the blood vessel density in the tumor mass and poor prognosis with chemoresistance in patients with various cancers (7–9). Furthermore, recent reports showing that anticancer agents were less active against VEGF-overexpressing tumors (10, 11) may support the idea that low-molecular drugs are not so effective in the treatment of solid tumors which are rich in blood vessels.

Our study thus far has several limitations about clarifying whether extensive angiogenesis in the tumor is an essential determinant for the susceptibility to NK012. In our ongoing study, we found that NK012 also has a striking antitumor activity against some hypovascular tumor models of human pancreatic cancer xenografts.[5] It also remains unclear whether NK012 possesses strong antitumor activity in other metastatic sites besides the lung. It is known that the EPR effect is affected by various permeability factors, such as bradykinin (12), nitric oxide (13), and various cytokines independent of VEGF and hypervascularity (14). Among solid tumors with rapid progression potential, irregularity occurs not only in blood flow and vascular density, but also in the vascular network and anatomic architecture (15, 16), suggesting that EPR effect may be predominantly promoted in rapid-progressive tumor phenotypes and influenced by organ-specific tumor microenvironment. Hoffman and coworkers (17, 18) have developed a technique of surgical orthotopic implantation (SOI) with more clinical features of systemic and aggressive metastases than our conventional animal models. Further preclinical studies using such models as SOI might clarify cancer phenotypes and metastatic organs to which we can apply NK012 more precisely.

The results of chemotherapy in RCCs have been disappointing, as indicated by the low response proportions. However, clinical trials using gemcitabine-containing regimens have been encouraging, with major responses occurring in 5% to 17% of patients (19, 20), suggesting the possibility that chemotherapy is promising as a modality for RCC therapy if anticancer agents can be selectively delivered, released, and maintained around tumor tissues. Our current report highlights the advantages of polymeric micelle-based drug carriers like NK012 as promising modalities for treatment, rather than prevention, of disseminated RCCs with abnormal vascular architecture. The results of our ongoing phase-I

[5] Y. Saito, M. Yasumaga, J. Kuroda, Y. Koga, and Y. Matsumura. Unpublished data.

clinical trial and future phase-II trials of NK012 in patients with advanced solid tumors including RCC might meet or even exceed our expectations.

## Acknowledgments

Received 12/10/2007; revised 1/25/2008; accepted 1/31/2008.

**Grant support:** Grant-in-aid from 3rd Term Comprehensive Control Research for Cancer, Ministry of Health, Labor and Welfare (Y. Matsumura) and Scientific Research on Priority Areas from the Ministry of Education, Culture, Sports, Science and Technology (Y. Matsumura).

The costs of publication of this article were defrayed in part by the payment of page charges. This article must therefore be hereby marked *advertisement* in accordance with 18 U.S.C. Section 1734 solely to indicate this fact.

We thank H. Miyatake and N. Mie for their technical assistance and K. Shiina for her secretarial assistance.

## References

1. Matsumura Y, Maeda H. A new concept for macromolecular therapeutics in cancer chemotherapy: mechanism of tumoritropic accumulation of proteins and the antitumor agent smancs. Cancer Res 1986;46:6387–92.
2. Yokoyama M, Miyauchi M, Yamada N, et al. Characterization and anticancer activity of the micelle-forming polymeric anticancer drug adriamycin-conjugated poly(ethylene glycol)-poly(aspartic acid) block copolymer. Cancer Res 1990;50:1693–700.
3. Kataoka K, Harada A, Nagasaki Y. Block copolymer micelles for drug delivery: design, characterization and biological significance. Adv Drug Deliv Rev 2001;47:113–31.
4. Matsumura Y, Hamaguchi T, Ura T, et al. Phase I clinical trial and pharmacokinetic evaluation of NK911, a micelle-encapsulated doxorubicin. Br J Cancer 2004;91:1775–81.
5. Hamaguchi T, Kato K, Yasui H, et al. A phase I and pharmacokinetic study of NK105, a paclitaxel-incorporating micellar nanoparticle formulation. Br J Cancer 2007;97:170–6.
6. Koizumi F, Kitagawa M, Negishi T, et al. Novel SN-38-incorporating polymeric micelles, NK012, eradicate vascular endothelial growth factor-secreting bulky tumors. Cancer Res 2006;66:10048–56.
7. Gasparini G, Harris AL. Clinical importance of the determination of tumor angiogenesis in breast carcinoma: much more than a new prognostic tool. J Clin Oncol 1995;13:765–82.
8. Takahashi Y, Kitadai Y, Bucana CD, Cleary KR, Ellis LM. Expression of vascular endothelial growth factor and its receptor, KDR, correlates with vascularity, metastasis, and proliferation of human colon cancer. Cancer Res 1995;55:3964–8.
9. Williams JK, Carlson GW, Cohen C, Derose PB, Hunter S, Jurkiewicz MJ. Tumor angiogenesis as a prognostic factor in oral cavity tumors. Am J Surg 1994;168:373–80.
10. Natsume T, Watanabe J, Koh Y, et al. Antitumor activity of TZT-1027 (Soblidotin) against vascular endothelial growth factor-secreting human lung cancer *in vivo*. Cancer Sci 2003;94:826–33.
11. Zhang L, Hannay JA, Liu J, et al. Vascular endothelial growth factor overexpression by soft tissue sarcoma cells: implications for tumor growth, metastasis, and chemoresistance. Cancer Res 2006;66:8770–8.
12. Matsumura Y, Maruo K, Kimura M, Yamamoto T, Konno T, Maeda H. Kinin-generating cascade in advanced cancer patients and *in vitro* study. Jpn J Cancer Res 1991;82:732–41.
13. Wu J, Akaike T, Hayashida K, et al. Identification of bradykinin receptors in clinical cancer specimens and murine tumor tissues. Int J Cancer 2002;98:29–35.
14. Maeda H, Fang J, Inutsuka T, Kitamoto Y. Vascular permeability enhancement in solid tumor: various factors, mechanisms involved and its implications. Int Immunopharmacol 2003;3:319–28.
15. Suzuki M, Takahashi T, Sato T. Medial regression and its functional significance in tumor-supplying host arteries. A morphometric study of hepatic arteries in human livers with hepatocellular carcinoma. Cancer 1987;59:444–50.
16. Skinner SA, Tutton PJ, O'Brien PE. Microvascular architecture of experimental colon tumors in the rat. Cancer Res 1990;50:2411–7.
17. An Z, Jiang P, Wang X, Moossa AR, Hoffman RM. Development of a high metastatic orthotopic model of human renal cell carcinoma in nude mice: benefits of fragment implantation compared to cell-suspension injection. Clin Exp Metastasis 1999;17:265–70.
18. Hoffman RM. Orthotopic metastatic mouse models for anticancer drug discovery and evaluation: a bridge to the clinic. Invest New Drugs 1999;17:343–59.
19. Rini BI, Vogelzang NJ, Dumas MC, Wade JL III, Taber DA, Stadler WM. Phase II trial of weekly intravenous gemcitabine with continuous infusion fluorouracil in patients with metastatic renal cell cancer. J Clin Oncol 2000;18:2419–26.
20. Nanus DM, Garino A, Milowsky MI, Larkin M, Dutcher JP. Active chemotherapy for sarcomatoid and rapidly progressing renal cell carcinoma. Cancer 2004;101:1545–51.

# Autosomal loci associated with a sex-related difference in the development of autoimmune phenotypes in a lupus model

*Naoko Misu[1,2], Mingcai Zhang[1], Shiro Mori[3], Tatsuhiko Miyazaki[4], Hiroshi Furukawa[1], Takeshi Sasaki[2], Masato Nose[4] and Masao Ono[1]*

[1] Department of Pathology, Tohoku University Graduate School of Medicine, Sendai, Japan
[2] Department of Rheumatology and Hematology, Tohoku University Graduate School of Medicine, Sendai, Japan
[3] Department of Oral Medicine and Surgery, Tohoku University Graduate School of Dentistry, Sendai, Japan
[4] Department of Pathology, Ehime University School of Medicine, Toon, Japan

Sex-related differences (SrD) are a general characteristic of human autoimmune diseases. There is an increasing body of evidence that suggests a link between sex-related hormones and autoimmune onsets. Here, through a genetic approach using a lupus mouse model, we attempted to show the involvement of genetic factors in the development of SrD in autoimmune diseases. Using MRL/lpr × (MRL/lpr × C57BL/6.Fas$^{lpr}$)F1 (MBN2) mice, the whole genome was searched to identify linkage loci to autoimmune phenotypes inherited from a lupus MRL/Mp.Fas$^{lpr}$ (MRL/lpr) strain of mice, which exhibits glomerulonephritis, splenomegaly and antinuclear autoantibody. The genome-wide association study confirmed four linkage loci on chromosomes 4, 7, 13, and 17. Furthermore, differential analyses performed using male and female groups of MBN2 mice revealed that two loci located on chromosomes 4 (41–72 cM, MRL/lpr allele) and 7 (4–21 cM, B6/lpr allele) were male specific and suppressed autoimmune phenotypes. Notably, the sum effect of the two loci adequately explained a range of SrD developed in the MBN2 mice. Our present findings suggest the presence of a male-predominant mechanism underlying the development of SrD in autoimmunity, depending on the effects of autosomal loci under an undefined male-specific condition.

Received 22/12/06
Revised 24/6/07
Accepted 2/8/07

[DOI 10.1002/eji.200637016]

**Key words:** Animal models · Autoimmunity · Genetics · Rheumatology

**Supporting information for this article is available at http://www.wiley-vch.de/contents/jc_2040/2007/37016_s.pdf**

## Introduction

Human autoimmune diseases occur due to interactions between genetic and environmental factors. Although these factors vary depending on every entity of autoimmune disease, female predominant onset is a general characteristic [1]. Indeed, the female to male incidence ratios for systemic lupus erythematosus (SLE), Sjögren's syndrome, Hashimoto disease, and rheumatoid arthritis (RA) are estimated to be 9:1, 9:1, 10:1, and 4:1, respectively. It is widely accepted that a crucial mechanism underlies the female susceptibility or male resistance to the development of an autoimmune disease.

Correspondence: Masao Ono, Department of Pathology, Tohoku University Graduate School of Medicine, 2–1 Seiryo, Aoba-ku, Sendai, Miyagi 980-8575, Japan
Fax: +81-22-717-8503
e-mail: onomasao@mail.tains.tohoku.ac.jp

Abbreviations: **GN:** glomerulonephritis · **LOD:** logarithm of odds · ***Marc4:*** male-specific autoimmune-resistant locus on chromosome 4 · ***Marc7:*** male-specific autoimmune-resistant locus on chromosome 7 · **MBF1:** (MRL/lpr × B6/lpr)F1 · **MBN2:** (MRL/lpr × MBF1)N2 · **QTL:** quantitative trait locus · **SpM:** splenomegaly · **SrD:** sex-related difference

Past studies conducted using animal autoimmune models have shown that an increased but non-toxic load of sex hormone [2–4], treatment with agonistic or antagonistic agent related to a sex hormone receptor [2, 4–6], or removal of sex glands [7, 8] affects the incidence or severity of autoimmune phenotypes. In humans, polymorphisms of genes encoding sex hormone receptors were shown to be associated with the onset of SLE [9] and RA [10, 11]. Transcriptional regulation of immunologically important genes by a sex hormone has been documented [12, 13]. These previous findings indicate the important role of sex hormones in the development of a sex-related difference (SrD) in autoimmune diseases.

The other lines of study have suggested a direct link between abnormality in sex chromosome and incidence of autoimmune disease. Congenital X-chromosome monosomy, *i.e.*, 45 XO Turner's syndrome, has been shown to render marked susceptibility to autoimmune disorders [14, 15]. A recent report demonstrated a high incidence of somatic X-chromosome monosomy in peripheral immune cells of patients with systemic sclerosis and autoimmune thyroiditis [16]. In this report, we have suggested the possible role of haploinsufficiency of X-linked genes in the onset of autoimmune diseases. These findings underscore the direct effect of sex chromosome-linked genes on the development of SrD in autoimmune diseases.

Autoimmune animal models have provided opportunities for understanding the genetic predisposition of autoimmune diseases. We have been using an autoimmune-prone strain of mice – MRL/Mp.*Fas*$^{lpr}$ (MRL/lpr) – to investigate the etiology of autoimmune disorders through genetic approaches. This strain was selected because it has the advantage of spontaneous development of a spectrum of autoimmune phenotypes that resemble human SLE. This strain carries a defective mutation in the *Fas* gene, denoted as *lpr* (for lymphoproliferation). The Fas protein is a cell-surface receptor that mediates apoptotic signals in activated lymphocytes. Therefore, the *lpr* mutation explains persistent autoimmune responses and lymphoproliferation due to the accumulation of abnormal CD4$^-$, CD8$^-$, CD45R (B220)$^+$, and Thy1$^+$ T cells in the MRL/lpr strain [17, 18]. On the other hand, it has been shown that other *lpr* congenic strains of mice – C3H/HeJ.*Fas*$^{lpr}$ and C57BL/6J.*Fas*$^{lpr}$ (B6/lpr) – barely develop autoimmune diseases [19–21], suggesting that the onset of the ultimate *lpr*-induced phenotypes depends on the genetic background of *lpr*. Genetic studies that relied on these *lpr*-related strains have provided explanations on the constitution of autoimmune susceptibility other than *lpr*.

Previous studies have suggested the lack of SrD in MRL/lpr mice [22–25]. In the early stage of this study, we carefully confirmed that MRL/lpr mice hardly display any SrD related to the severity of autoimmune phenotypes, including glomerulonephritis (GN), splenomegaly (SpM), and autoantibody to nuclear antigens (ANA). In contrast, the descendent strains – (MRL/lpr × B6/lpr)F1 (MBF1) and (MRL/lpr × MBF1)N2 (MBN2) – were found to exhibit significant SrD, suggesting the presence of strain-specific genetic factors responsible for the development of SrD in the MBF1 and MBN2 strains. Here, we attempted to identify sex-specific loci to elucidate the development of SrD in the MBN2 model. Differential genetic analyses performed using the male and female groups of MBN2 mice revealed two male-specific autosomal loci associated with the suppression of autoimmune phenotypes. These findings suggest the presence of a male-specific mechanism underlying the SrD in autoimmune disorders.

## Results

### Histopathological characterization of glomerulonephritis in MBN2 mice

Fully developed GN in the MRL/lpr and MBN2 mice was similarly characterized by increases in the cellular and matrix components of the glomerulus (data not shown). As described in the *Materials and methods*, two different indexes – cellular and matrix grades – were used to quantify a pathological change in the glomerulus in the MBN2 mice independently. We observed a significant correlation between the two grades of GN (Supporting Information Fig. 1). This finding suggests the presence of a mutual dependence of the cellular and matrix proliferations in the development of GN in the MBN2 mice. Hereafter, we adopted a $\log_{10}$-transformed index based on the two grades as an individual GN index.

### Strain-specific onset of SrD in autoimmune phenotypes

Four autoimmune phenotypes including GN, SpM, ANA of IgM class, and ANA of IgG class were quantified in the MRL/lpr, B6/lpr, MBF1, and MBN2 mice. The results showed that the MRL/lpr mice developed all the phenotypes without any evidence of SrD (Table 1). On the other hand, the MBN2 mice developed all the phenotypes with significant SrD. The MBF1 and B6/lpr mice also exhibited significant SrD for some phenotypes. The severity of any of these phenotypes in the male and female groups was found to be normally distributed (Fig. 1). These findings suggest the contribution of complex genetic factors, including B6/lpr-derived factor(s), to the onset of SrD in MBF1 and MBN2 mice.

**Table 1.** Severity of autoimmune phenotypes in male and female groups of MRL/lpr, B6/lpr, MBF1 and MBN2 mice[a)]

| strain | group | trait[b)] | | | | | | | |
|---|---|---|---|---|---|---|---|---|---|
| | | GN $\log_{10}$ index | | ANA-IgM titer score | | ANA-IgG titer score | | SpM mg | |
| MRL/lpr | total | 2.29 (0.198, 23) | | 2.80 (0.847, 30) | | 4.90 (0.803, 30) | | 557 (284, 28) | |
| | male | 2.25 (0.182, 12) | | 2.75 (0.860, 12) | | 5.00 (0.852, 12) | | 514 (180, 13) | |
| | female | 2.33 (0.213, 11) | | 2.83 (0.857, 18) | | 4.83 (0.786, 18) | | 594 (353, 15) | |
| B6/lpr | total | 0.803 (0.414, 25) | | 0.696 (0.635, 23) | | 2.48 (0.70, 23) | | 213 (98.0, 17) | |
| | male | 0.648 (0.234, 9) | | 0.688 (0.704, 16) | | 2.50 (0.730, 16) | | 132 (34.5, 9) | *** |
| | female | 0.891 (0.471, 16) | | 0.714 (0.488, 7) | | 2.43 (0.535, 7) | | 305 (51.7, 8) | |
| MBF1[c)] | total | 1.52 (0.554, 56) | | 1.94 (1.15, 53) | | 3.87 (0.680, 53) | | 725 (338, 56) | |
| | male | 1.13 (0.445, 22) | *** | 1.77 (1.11, 22) | | 3.46 (0.583, 22) | *** | 482 (221, 22) | *** |
| | female | 1.76 (0.475, 34) | | 2.06 (1.18, 31) | | 4.16 (0.596, 31) | | 881 (308, 34) | |
| MBN2[d)] | total | 1.51 (0.518, 348) | | 1.67 (1.17, 348) | | 3.39 (1.32, 348) | | 549 (440, 348) | |
| | male | 1.38 (0.480, 189) | *** | 1.49 (1.25, 189) | * | 2.99 (1.30, 189) | *** | 460 (458, 189) | *** |
| | female | 1.67 (0.520, 159) | | 1.88 (1.01, 159) | | 3.87 (1.17, 159) | | 656 (394, 159) | |

[a)] Value denotes a mean (S.D., number of mice) of trait index. Difference of averages between male and female groups were estimated by Student's *t*-test. $*p < 0.05$; $***p < 0.0001$.

[b)] GN, glomerulonephritis; ANA, antinuclear autoantibody; SpM, splenomegaly.

[c)] (MRL/lpr × B6/lpr) F1.

[d)] MRL/lpr × (MRL/lpr × B6/lpr) N2.

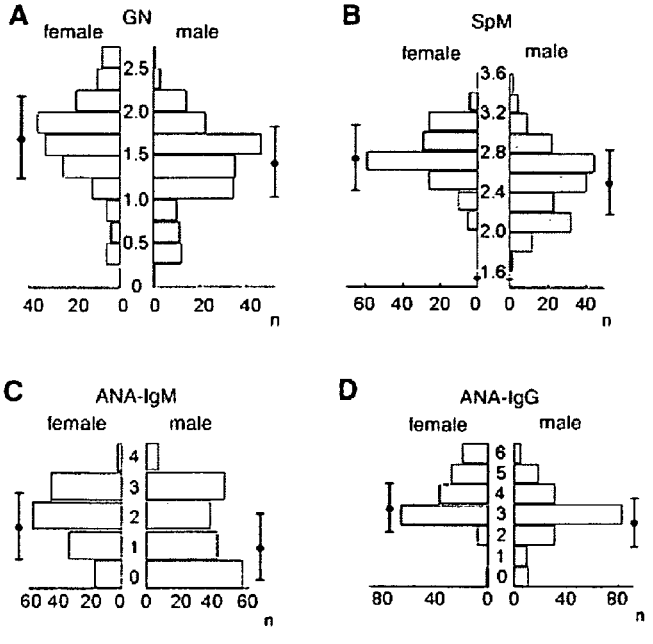


**Figure 1.** SrD in severity-stratified distribution of the autoimmune traits in MBN2 mice. (A) GN index represents the disease severity, estimated by $\log_{10}$ [(mean of cellular grades) + (mean of matrix grades)]. The distribution of $\log_{10}$-transformed GN indexes was estimated as normal. (B) SpM index denotes $\log_{10}$-transformed spleen weight. (C, D) Titers of ANA were determined by immunofluorescence analysis. A diagonal dot with lines by each bar graph indicates a mean with SD. For all the indexes, difference between the male and female groups is statistically significant.

## Identification of four loci associated with autoimmune phenotypes

By genome-wide screening, we evaluated the difference in the average severity of each autoimmune phenotype between two subgroups of 95 MBN2 mice that were sorted depending on the genotype at every microsatellite position: MRL/MRL homozygote and MRL/B6 heterozygote. The *t* test ($p<0.05$) preliminarily qualified nine regions on chromosomes 1, 2, 4, 5, 7, 10, 11, 13, and 17 as candidate loci for any of the autoimmune phenotypes (Supporting Information Fig. 2). We next examined other approximately 100 MBN2 mice that were randomly selected, and re-evaluated the preliminary nine loci using the accumulated data in the same manner, except that the threshold *p* value for acceptance was $<0.02$. At this stage, we differentially examined the male and female groups. Four regions on chromosomes 4, 7, 13, and 17 were estimated as significant. Finally, association studies and quantitative trait locus (QTL) analyses performed using 348 MBN2 mice confirmed their statistical significance (Table 2). Analysis with relative spleen weight (mg/g of body weight) reproduced extremely similar results.

 

**Table 2.** Association of microsatellite genotypes[a] and autoimmune phenotypes in MBN2 mice

| trait[b] | chr. | marker | position | Male | | | Female | | |
|---|---|---|---|---|---|---|---|---|---|
| | | | | mean (S.D., number of mice) | | $p$[c] | mean (S.D., number of mice) | | $p$[c] |
| | | | cM | MM | MB | | MM | MB | |
| GN ($log_{10}$ index) | 4 | D4Mit124 | 57.4 | 1.24 (0.50, 89) | 1.52 (0.42, 100) | **0.00004**** | 1.59 (0.56, 85) | 1.76 (0.46, 74) | 0.0050 |
| | | D4Mit71 | 61.9 | 1.43 (0.56, 85) | 1.60 (0.46, 104) | **0.00023*** | 1.61 (0.56, 90) | 1.74 (0.46, 69) | 0.11 |
| | 7 | D7Mit57 | 4 | 1.50 (0.46, 98) | 1.26 (0.47, 91) | **0.00082*** | 1.67 (0.55, 82) | 1.69 (0.55, 77) | 0.83 |
| | | D7Mit267 | 11 | 1.48 (0.48, 99) | 1.28 (0.46, 90) | 0.0043 | 1.69 (0.56, 86) | 1.68 (0.51, 73) | 0.95 |
| | | D7Mit155 | 15 | 1.47 (0.48, 99) | 1.29 (0.46, 90) | 0.0087 | 1.69 (0.56, 88) | 1.65 (0.48, 71) | 0.62 |
| | 13 | D13Mit24 | 43 | 1.36 (0.45, 85) | 1.41 (0.51, 104) | 0.48 | 1.79 (0.54, 76) | 1.56 (0.48, 83) | 0.0046 |
| | | D13Mit147 | 49 | 1.37 (0.45, 87) | 1.40 (0.50, 102) | 0,67 | 1.79 (0.49, 74) | 1.56 (0.52, 85) | 0.0048 |
| | 17 | D17Mit197 | 9.65 | 1.42 (0.44, 95) | 1.35 (0.51, 94) | 0.35 | 1.70 (0.51, 84) | 1.64 (0.53, 75) | 0.47 |
| | | D17Mit214 | 18.7 | 1.41 (0.46, 97) | 1.36 (0.50, 92) | 0.45 | 1.70 (0.51, 83) | 1.63 (0.54, 76) | 0.41 |
| ANA-IgM (titer score) | 4 | D4Mit124 | 57.4 | 1.21 (1.10, 89) | 1.74 (1.33, 100) | 0.0037 | 1.80 (1.02, 85) | 1.99 (1.00, 74) | 0.25 |
| | | D4Mit71 | 61.9 | 1.17 (1.13, 85) | 1.76 (1.29, 104) | **0.0010*** | 1.76 (1.04, 90) | 2.06 (0.95, 69) | 0.062 |
| | 7 | D7Mit57 | 4 | 1.77 (1.27, 98) | 1.20 (1.18, 91) | **0.0017*** | 1.94 (1.02, 82) | 1.83 (1.01, 77) | 0.60 |
| | | D7Mit267 | 11 | 1.79 (1.28, 99) | 1.17 (1.14, 90) | **0.00057*** | 1.92 (1.00, 86) | 1.85 (1.04, 73) | 0.85 |
| | | D7Mit155 | 15 | 1.77 (1.28, 99) | 1.19 (1.16, 90) | **0.0014*** | 1.93 (1.00, 88) | 1.83 (1.04, 71) | 0.70 |
| | 13 | D13Mit24 | 43 | 1.73 (1.31, 85) | 1.30 (1.17, 104) | 0.018 | 1.93 (1.02, 76) | 1.84 (1.00, 83) | 0.57 |
| | | D13Mit147 | 49 | 1.67 (1.27, 87) | 1.34 (1.22, 102) | 0.077 | 1.97 (0.96, 74) | 1.81 (1.01, 85) | 0.32 |
| | 17 | D17Mit197 | 9.65 | 1.63 (1.20, 95) | 1.35 (1.29, 94) | 0.12 | 1.92 (0.92, 84) | 1.85 (1.11, 75) | 0.70 |
| | | D17Mit214 | 18.7 | 1.63 (1.21, 97) | 1.35 (1.29, 92) | 0.12 | 1.92 (0.91, 83) | 1.86 (1.12, 76) | 0.71 |
| ANA-IgG (titer score) | 4 | D4Mit124 | 57.4 | 2.73 (1.21, 89) | 3.22 (1.34, 100) | 0.0089 | 3.77 (1.09, 85) | 4.00 (1.25, 74) | 0.21 |
| | | D4Mit71 | 61.9 | 2.68 (1.24, 85) | 3.24 (1.30, 104) | **0.0030*** | 3.70 (1.16, 90) | 4.10 (1.15, 69) | 0.031 |
| | 7 | D7Mit57 | 4 | 3.20 (1.17, 98) | 2.76 (1.40, 91) | 0.018 | 4.00 (1.16, 82) | 3.74 (1.16, 77) | 0.50 |
| | | D7Mit267 | 11 | 3.20 (1.16, 99) | 2.76 (1.41, 90) | 0.018 | 3.95 (1.16, 86) | 3.78 (1.18, 73) | 0.67 |
| | | D7Mit155 | 15 | 3.18 (1.16, 99) | 2.78 (1.41, 90) | 0.032 | 3.96 (1.17, 88) | 3.77 (1.16, 71) | 0.53 |
| | 13 | D13Mit24 | 43 | 3.20 (1.29, 85) | 2.82 (1.29, 104) | 0.044 | 3.83 (1.19, 76) | 3.92 (1.15, 83) | 0.74 |
| | | D13Mit147 | 49 | 3.15 (1.36, 87) | 2.85 (1.24, 102) | 0.12 | 3.92 (1.13, 74) | 3.83 (1.20, 85) | 0.65 |
| | 17 | D17Mit197 | 9.65 | 3.08 (1.26, 95) | 2.89 (1.34, 94) | 0.31 | 3.68 (1.05, 84) | 4.08 (1.25, 75) | 0.025 |
| | | D17Mit214 | 18.7 | 3.10 (1.26, 97) | 2.87 (1.34, 92) | 0.22 | 3.69 (1.08, 83) | 4.08 (1.23, 76) | 0.034 |
| SpM ($log_{10}$ mg) | 4 | D4Mit124 | 57.4 | 2.42 (0.34, 89) | 2.60 (0.34, 100) | **0.00039*** | 2.70 (0.26, 85) | 2.79 (0.25, 74) | 0.033 |
| | | D4Mit71 | 61.9 | 2.42 (0.35, 85) | 2.59 (0.34, 104) | **0.0011*** | 2.70 (0.27, 90) | 2.80 (0.24, 69) | 0.012 |
| | 7 | D7Mit57 | 4 | 2.59 (0.34, 98) | 2.43 (0.35, 91) | **0.0025*** | 2.76 (0.27, 82) | 2.73 (0.26, 77) | 0.52 |
| | | D7Mit267 | 11 | 2.58 (0.34, 99) | 2.44 (0.35, 90) | 0.0060 | 2.76 (0.27, 86) | 2.72 (0.25, 73) | 0.41 |
| | | D7Mit155 | 15 | 2.58 (0.35, 99) | 2.45 (0.35, 90) | 0.012 | 2.76 (0.27, 88) | 2.72 (0.25, 71) | 0.27 |
| | 13 | D13Mit24 | 43 | 2.58 (0.39, 85) | 2.46 (0.31, 104) | 0.013 | 2.81 (0.28, 76) | 2.68 (0.22, 83) | **0.0020*** |
| | | D13Mit147 | 49 | 2.59 (0.39, 87) | 2.45 (0.30, 102) | 0.0055 | 2.80 (0.28, 74) | 2.69 (0.23, 85) | 0.0073 |
| | 17 | D17Mit197 | 9.65 | 2.60 (0.39, 95) | 2.43 (0.30, 94) | **0.0011*** | 2.80 (0.28, 84) | 2.68 (0.22, 75) | 0.0060 |
| | | D17Mit214 | 18.7 | 2.60 (0.39, 97) | 2.42 (0.29, 92) | **0.00051*** | 2.80 (0.29, 83) | 2.68 (0.22, 76) | **0.0012*** |

[a] MM and MB denote MRL/MRL homozygote and MRL/B6 heterozygote, respectively.
[b] GN, glomerulonephritis; ANA, antinuclear antibody; dsDNA, anti-double stranded DNA antibody; SpM, splenomegaly.
[c] Student's $t$-test. * $p < 0.0034$ (suggestive); ** $p < 0.0001$ (significant).

## Male-predominant autoimmune-resistant locus on chromosome 4

Data from the 348 MBN2 mice revealed male-specific associations of the MRL/lpr allele with all the autoimmune phenotypes examined at *D4Mit124* (57.4 cM) and/or *D4Mit71* (61.9 cM). These associations were observed in the male group; the phenotypes of the MRL/lpr allele demonstrated a recessive resistance inheritance (Table 2). The QTL analyses of the male group demonstrated a single logarithm of odds (LOD) peak beyond the threshold of significance for GN, SpM, ANA-IgM, and ANA-IgG at positions 57.3, 59.4, 61.7, and 61.9 cM, respectively (Fig. 2). In contrast, such common associations were not observed in the female group (Fig. 2). Here, we designated the linkage interval that included all significant QTL points (41–72 cM) as *Marc4* (for male-specific autoimmune-resistant locus on chromosome 4).

## Male-predominant autoimmune-resistant locus on chromosome 7

Suggestive associations of the genotypes with GN, ANA-IgM, and SpM were observed at *D7Mit57* (4 cM) or *D7Mit267* (11 cM) in the male group; the phenotypes of the B6/lpr allele demonstrated a dominant resistance inheritance (Table 2). Although these markers also showed tendencies for association with ANA-IgG, the tendencies were not statistically supported. The QTL analyses of the male group demonstrated a single LOD peak beyond the threshold of significance for GN, ANA-IgM, and SpM at positions 5.8, 9.6, and 4.7 cM, respectively (Fig. 3). Here, we designated the linkage interval that included all significant QTL points (4–21 cM) as *Marc7* (for male-specific autoimmune-resistant locus on chromosome 7).

## Autoimmune susceptibility loci on chromosomes 13 and 17

We detected two suggestive associations of the genotypes with SpM at *D13Mit24* (43 cM) and *D17Mit214* (18.7 cM) (Table 2). The association at *D13Mit24* was observed only in the female group; however, the QTL analyses for SpM demonstrated a single LOD peak between *D13Mit24* and *D13Mit147* (49 cM) in both male and female groups (Fig. 3), suggesting that this locus is not exclusively female predominant. The association at *D17Mit214* was observed without any sex-related predominance (Table 2). This was supported by the significant QTL that included this marker position (Fig. 3). A significant QTL for GN was observed between *D13Mit24* and *D13Mit147* in the female group (Fig. 3).

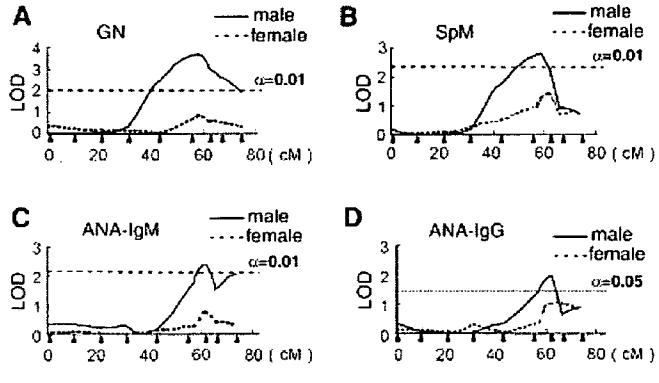


**Figure 2.** Plots of LOD scores of QTL on chromosome 4 for an autoimmune trait in MBN2 mice. The genetic positions (cM) of microsatellite markers used in QTL analysis are indicated on horizontal axis with arrowheads. A peak of LOD for GN (A), SpM (B), ANA-IgM (C), ANA-IgG (D) was identified at the position 57.3, 59.4, 61.7, and 61.9 cM, respectively. We adopted interval mapping in the Windows QTL Cartographer (V2.5) software. Horizontal broken and dotted line lines indicate the threshold level of statistic significance at α=0.01 and α=0.05, respectively.

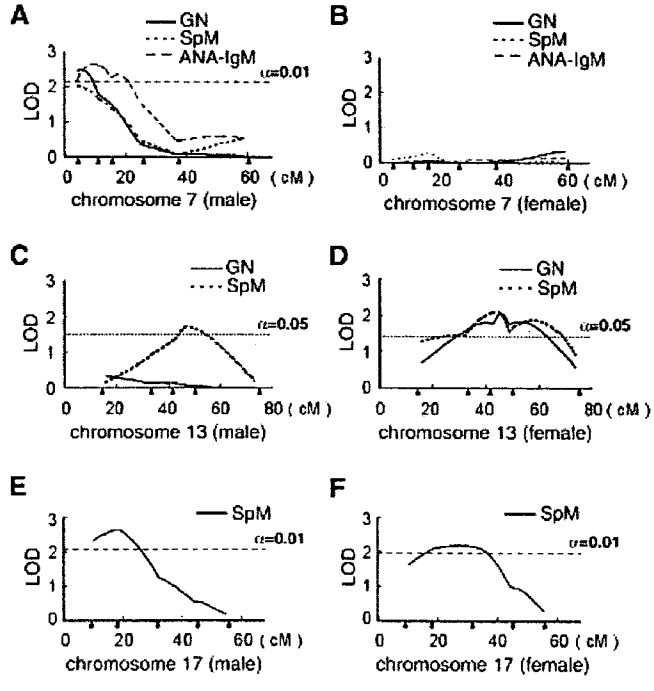


**Figure 3.** Plots of LOD scores of QTL for an autoimmune trait on chromosomes 7, 13, and 17. The genetic positions (cM) of microsatellite markers used in QTL analysis are indicated on horizontal axis with arrowheads. The male and female results are shown on the left and right side, respectively. (A) Peaks of LOD for GN, ANA-IgM, and SpM were identified in the male group of MBN2 mice at the position 5.8, 9.6, and 4.7 cM, respectively, on chromosome 7. (B) No significant peak was observed in the female group on this chromosome. The genetic linkages to SpM and GN were observed on chromosome 13 (C, D) and 17 (E, F). The threshold levels are indicated as in Fig. 2.

### Effects of *Marc4* and *Marc7* on SrD in autoimmune phenotypes

The male and female groups of MBN2 mice were each divided into four subcohorts based on the genotype combinations of *D4Mit124* and *D7Mit57*, which are included in *Marc4* and *Marc7*, respectively. The averages and SD of the trait index of each subcohort are summarized in Table 3. Significant variance in the average indexes among the four subcohorts was evident in the male group ($p<0.001$). Except the effect of *Marc4* on SpM, each locus exhibited a significant effect on the SrD for every autoimmune phenotype of interest in the male group. The two loci exhibited an additive suppressive effect on these phenotypes, which was accountable for the entire range of SrD developed in the MBN2 mice. To evaluate the interaction between two QTL of interest, we adopted the R/qtl program [26]. The strength of the interaction between two QTL was estimated by the LOD score in the interaction mode. An interaction was not observed for any two QTL identified on chromosomes 1, 4, 7, 13, and 17, which included *Marc4* and *Marc7*. The results on *Marc4* and *Marc7* are presented in Table 4.

## Discussion

Female preponderance in the incidence of human autoimmune diseases implies that sex-specific conditions yield susceptibility to autoimmune diseases. It has been principally considered that a sex hormone directly or indirectly affects immune cell functions and that this effect results in autoimmune reaction enhancement in females or its suppression in males. The present study revealed two male-specific autosomal loci – *Marc4* and *Marc7* – that dominated the suppression of autoimmune phenotypes in the present autoimmune model. These findings suggest a male-specific mechanism underlying SrD in the onset of autoimmune diseases. Concurrently, a new question arose on the interaction between sex hormones and these loci. Although this should be investigated by further studies, the effect of *Marc4* cannot be explained by this interaction.

There are inconsistent facts that MBN2 mice show remarkable SrD in autoimmune phenotypes, while their ancestral MRL/lpr mice do not show significant SrD. Past studies have readily confirmed little SrD in the autoimmune phenotypes of an MRL/lpr strain [22–25]. Here, a question that arose was why the male-specific

**Table 3.** Genetic effects of *Marc4* and *Marc7* on sex-related difference in autoimmune phenotypes[a)]

| trait[b)] | sex | | subcohorts by *Marc4*/*Marc7* genotypes[d)] | | | |
|---|---|---|---|---|---|---|
| | | all | MM/MM | MM/MB | MB/MM | MB/MB |
| GN ($log_{10}$ index) | male[§ c)] | 1.38 (0.48, 189)*** | 1.34 (0.46, 37)* | 1.16 (0.52, 52)*** | 1.59 (0.44, 61) | 1.40 (0.36, 39)*** |
| | female | 1.67 (0.52, 159) | 1.64 (0.59, 44) | 1.55 (0.53, 41) | 1.70 (0.47, 38) | 1.82 (0.46, 36) |
| ANA-IgM (titer score) | male[§] | 1.49 (1.25, 189)*** | 1.41 (1.17, 37)* | 1.08 (1.04, 52)** | 1.98 (1.28, 61) | 1.36 (1.33, 39)* |
| | female | 1.88 (1.01, 159) | 1.91 (1.03, 44) | 1.68 (1.01, 41) | 1.97 (1.03, 38) | 2.00 (0.99, 36) |
| SpM (mg) | male[§] | 460 (458, 189)*** | 443 (578, 37) | 326 (325, 52)** | 592 (484, 61) | 447 (398, 39)** |
| | female | 656 (394, 159) | 646 (450, 44) | 565 (366, 41) | 726 (401, 38) | 703 (331, 36) |

a) Value denotes a mean (S.D., number of mice) of the indicated trait index. Difference of averages between male and female groups was estimated by Student's t-test. * $p < 0.05$; ** $p < 0.01$; *** $p < 0.001$.
b) GN, glomerulonephritis; ANA, antinuclear autoantibody; SpM, splenomegaly.
c) Variance among the genotype subcohorts was statistically evaluated by one-way ANOVA. § $p < 0.01$.
d) MM and MB denote MRL/MRL homozygote and MRL/B6 heterozygote, respectively.

**Table 4.** Interaction *Marc4* and *Marc7* in the male group[a)]

| trait[b)] | locus1[c)] | locus2[d)] | lod.full[e)] | lod.add[e)] | lod.int[e)] |
|---|---|---|---|---|---|
| GN | c4 (50 cM) | c7 (9 cM) | 5.36 (4.79)* | 5.29 (3.58)* | 0.08 (3.07) |
| SpM | c4 (50 cM) | c7 (4 cM) | 4.11 (4.59) | 4.09 (3.46)* | 0.02 (2.62) |
| ANA-IgM | c4 (55 cM) | c7 (19 cM) | 4.45 (3.91)* | 4.24 (3.11)* | 0.21 (2.83) |

a) Value represents a calculated LOD with a threshold in parenthesis ($\alpha = 0.05$). * $p < 0.05$.
b) GN, glomerulonephritis; ANA, antinuclear antibody; SpM, splenomegaly.
c) Calculated position of maximum LOD on chromosome 4.
d) Calculated position of maximum LOD on chromosome 7.
e) lod.full, LOD score in the full mode; lod.add, LOD score in the additive mode; lod.int, LOD score in the interactive mode.

suppression by *Marc4* had attenuated in the male mice of this strain. A possible answer is that *Marc4* requires interaction with a B6/lpr-derived factor to exert its effect on SrD. *Marc7* could be a candidate B6/lpr-derived factor. However, as shown in Table 4, *Marc7* had no epistatic effect on *Marc4*, suggesting that another B6-derived factor activates *Marc4*. We further searched chromosomes 1, 13, and 17 with genotyping data obtained from all MBN2 mice for another epistatic locus to *Marc4*, but no such locus was detected (data not shown). We cannot rule out a possibility that an epistatic autosomal locus exists and that this locus is so weakly associated with the examined autoimmune phenotypes that it was overlooked in our genome-wide screening. Alternatively, another possibility is that a B6/lpr-derived Y chromosome is epistatic to *Marc4*. In this regard, there is a noteworthy report that documented SrD in the incidence of GN observed in two closely related backcross mice – MRL/lpr × (B6/lpr × MRL/lpr)F1 (BMN2) and MBN2 [21]. This report showed that MBN2 mice developed a clear tendency toward SrD, whereas the BMN2 mice developed little SrD. These findings have supported the contribution of the B6/lpr-derived Y chromosome or MRL/lpr-derived X chromosome to the development of SrD.

A mutation in the mitochondrial genome and abnormalities in sex chromosome, *i.e.*, Turner's syndrome and Klinefelter's syndrome, have been shown to predispose humans to autoimmune disorders. For example, mitochondrial DNA mutations cause a type of non-insulin-dependent diabetes and encephalomyelitis with an autoimmune etiology [27, 28]; Turner's syndrome and Klinefelter's syndrome predispose the patients to autoimmune thyroid disease and SLE-like disease, respectively [14, 15, 29, 30]. Some mitochondria-genomic disorders critically involve the female population [28]. Although the mechanism for this female preponderance remains unclear, this fact suggests a link between a mitochondrial phenotype and female gender. The association of sex chromosome abnormalities with the onset of autoimmune disease is indirect evidence that a sex chromosome directly contributes to autoimmune disease onset. Previous studies on this line have suggested a pathogenic impact of the number of an unidentified X allele on an autoimmune disease. This could be further implicated in the mechanism underlying SrD in autoimmune disease onset. The mitochondria and X chromosome in the present male MBN2 mice are derived from MRL/lpr females. Therefore, these genetic components are not implicated in the mechanism of male-specific autoimmune suppression that was observed in the MBN2 but not in the MRL/lpr mice. Instead, a direct role of the Y chromosome is considered. Although little is known about this role, a recent study conducted using a model for experimental allergic encephalomyelitis has demonstrated this role of Y chromosome [31]. The Y-chromosome consomic strain, a murine model, will provide an answer to this question.

A number of studies performed using murine autoimmune models have documented autoimmune-linkage loci. *Marc4* and *Marc7* overlap well with some of these loci associated with SpM [32, 33], GN [34–38], vasculitis [39], anti-dsDNA [32, 36, 37], or mortality [33]. Sex-related preponderance was not examined for these loci. It is particularly noteworthy that a study conducted using (MRL/lpr × B6/lpr)F2 mice demonstrated two resistant loci MRL/lpr and B6/lpr alleles associated with SpM and anti-dsDNA; these alleles correspond to *Marc4* and *Marc7*, respectively [32].

There are genetic or functional implications of the genes included in *Marc4* and *Marc7* in the pathogenic context of autoimmune diseases. For example, the *lck* gene (60 cM of chromosome 4), which encodes for an src-family tyrosine kinase and plays a role in TCR signal transduction, was recently found to be down-regulated in the T cells of patients with SLE [40]. The *c1q* gene (66.1 cM of chromosome 4) encoding C1q, a complement component, is believed to be involved in the pathogenesis of SLE because it has been reported that approximately 90% of patients with congenital defects in C1q develop SLE early [41]. C1q-deficient mice were shown to develop autoantibody and GN [42]. A genetic polymorphism in the promoter region of the *c1qa* gene was identified in a lupus NZB strain [43]. The platelet-activating factor (PAF) receptor (*ptafr*, 62.4 cM on chromosome 4) has been suggested to contribute to the pathogenesis of GN through platelet activation. Administration of the PAF receptor antagonist flaxseed ameliorated proteinuria and SpM in MRL/lpr mice [44]. Patients with SLE demonstrated decreased activity of PAF acetylhydrolase, which is a degradation enzyme of PAF [45].

In the proximal region of chromosome 7, receptor *cd22* (9 cM) that regulates B cell survival and activation is underscored as a candidate that affects *Marc7* as previous studies indicated the association between a CD22 allotype ($cd22^a$) and autoimmune disease onset in a *Yaa*-related autoimmune condition [46]. MRL/lpr represents lupus-prone $cd22^a$ that is different from B6/lpr ($cd22^b$) (Nose *et al.*, unpublished data). In humans, the therapeutic use of anti-CD22 is under trial for the treatment of SLE [47].

This study revealed two loci on chromosomes 13 and 17 that yield susceptibilities to GN and SpM, and only SpM, respectively, in the MBN2 mice. These loci also overlap with previously defined loci in other autoimmune models [33, 34, 36, 37, 48]. Past studies have highly implicated the chromosome 17 interval because it includes the *H-2* region. This study, however, could not

 